



TabSat: Theoretical Design Approach of Distributed Femto satellite system for forest fire monitoring

Supervised by Mr. Akshay Choudari, Mr. Vishnuvardhan
Shaktibala and Ms. Rashika SN

Research Internship Project Report- *Team Femoyer*

October, 2020

A Submitted to SSERD as Final Internship Report.

Acknowledgements

We would like to acknowledge the support provided to us by **SSERD - Society for Space Education Research and Development** for the successful completion of the Research Internship.

We owe great many thanks to **Mr. Akshay Choudhari**, **Mr. Vishnuvardhan Shaktibala** and **Ms. Rashika SN**, for their immense help in the literature survey and the conception without which the research would not have seen the light of the day. We sincerely thank them for providing continuous guidance and suggestions which paved the way for smooth progress and fruitful culmination of the research.

We thank **Mr. Sujay Sreedhar** and **Ms. Nikhitha C**, Co-founders of SSERD for the allotment of the topic Femtosatellites and their immense dedication towards supporting the fruition of this research.

We thank **Ms. Rutuja Attal**, for volunteering as our team coordinator and assisting us with conundrums and impediments faced during the research.

Abstract

Femto satellite has been an extensive area of research and interest for many space professionals. Over the past years, many missions like Kicksat, PCBSAT, 50 dollar Sat have tried to explore the depths of this technology for real-time applications. The aim of this research work is to provide a theoretical design of a cluster of distributed femto satellites along with the deployer (hub design) for monitoring forest fire using Remote Sensing .

The entire project was divided into two parts: **I.** The femto satellite and **II.** The deployer. The first part encompassing the design of the femto satellite which was undertaken using the software **fusion 360**, without a circuitry development. The orbit selected is the **Sun Synchronous Orbit** with an inclination of 98.57° , with one cluster comprising three femto satellites. The orbital parameters such as eccentricity, inclination, argument of perigee, Right Ascension of the Ascending Node and true anomaly were measured using a **matlab code** and the orbit as a whole was also simulated, using the software: **Systems Tool Kit**.

The second part predominantly involves the design of deployer based on the femto satellite dimensions, carried forward using the **PTC Creo** software. The entire model was then exported to the **ANSYS** software in order to carry out the simulation of the same.

To the Future of Space Research.

Contents

1	Introduction	1
1.1	Mission Overview	1
1.2	Aims	2
1.3	Objectives	3
2	Background & Literature Overview	4
2.1	Survey	4
3	Astrodynamic Subsystem	6
3.1	Orbit Selection	6
3.1.1	Why Sun-Synchronous orbit?	6
3.2	Computer Program for Predicting Orbital Events	8
3.3	The Constellation of Femto satellites and HUB	13
3.4	Data Visualization of Orbital Parameters	14
3.5	Calculations of Hohmann Orbit Transfer	16
3.6	Data Visualization of Gravity Perturbed Hohmann Orbit Transfer	18
3.7	Computer Program for Solving Gravity Perturbed Trajectory Problem and for Targeting the Orbit	20
3.8	Computer Program for Analysis of Relative Motion Trajectories between two Femto satellites	25
3.9	Data Visualization of Relative Motion Trajectories between two Femto satellites	28
3.10	Maximization of Orbital Inclination	29
3.11	Orbit Design and Simulation	30

4 Payload Subsystem	31
4.1 Workflow	31
5 Electrical Subsystem	36
5.1 Electrical Power Subsystem	36
5.1.1 Literature Survey	37
5.2 Objectives	37
5.3 Power Budget: Femto Satellite	38
5.3.1 Power required by all subsystems	38
5.3.2 Power Generation	39
5.3.3 Power Storage	42
5.3.4 Power Distribution	43
5.3.5 Power Regulation and Control	43
5.3.6 Finalized Components/Design for Power System in Femto Satellite	44
5.4 Power Budget: HUB	46
5.4.1 Power Requirement of all Subsystems	46
5.4.2 Power Generation	47
5.4.3 Power Storage	51
5.4.4 Power Distribution	51
5.4.5 Power Regulation And Control	52
5.4.6 Finalized Components/Design for Power System in HUB	52
5.5 Attitude Determination and Control System	
For Femto satellite	56
5.5.1 Altitude Determination System: ADS	56
5.5.2 Altitude Control System: ACS	59
5.5.3 Algorithm	62
5.6 Attitude Determination and Control System	
For Hub	64
5.7 Position Determination System	
For Femto satellite	67
5.8 Position Determination System	
For Hub	70
6 Communication Subsystem	73
6.1 Communication systems	73
6.2 Objectives	73
6.3 Communication Flow	74

6.3.1	Matched filtering:	74
6.3.2	Aspects	74
6.4	Components	75
6.4.1	Criteria for the selection of the components	75
6.4.2	Femto-Satellite	76
6.4.3	Hub	77
6.5	Link Budget	78
6.5.1	Link budget calculations	78
7	Structural Design	80
7.1	Component design	80
7.1.1	Final design	89
7.2	Mass and Volume budget	90
8	Deployer-The Hub	91
8.1	TabSat Mission Requirements	91
8.2	6U Dispenser Interface	92
8.3	Requirements	92
8.3.1	General requirements	92
8.3.2	Mechanical Requirements	93
8.3.3	Electrical Requirements	94
8.3.4	Operational Requirements	95
8.3.5	Testing Requirements	95
8.3.6	Deployment and Spring Design	96
8.3.7	Deployment of the Solar Panels	98
8.4	Design Overview	99
8.4.1	Design of Magnetic Torquers for Attitude Control	100
8.5	Structural Requirements	101
8.6	Material	102
8.7	Analysis	103
8.7.1	Dynamical Analysis	103
8.7.2	Electromagnetic Interference Analysis	104
8.7.3	Impact of Magnetic Torquer on the Magnetometer	105
9	Propulsion Subsystem	108
9.1	Micro-propulsion system for HUBsat	108
10	Conclusion	112

10.1 Achieved Aims and Objectives	112
10.2 Critiques and limitations	113
10.3 Future Work	113
References	115

List of Figures

1.1	Schematics of Mission TabSat	2
1.2	Objectives.	3
3.1	Sun-synchronous Polar Orbit (11)	7
3.2	Eccentricity	14
3.3	Inclination	15
3.4	Argument of Perigee	15
3.5	Longitude of Ascending Node	15
3.6	Semi-major axis	16
3.7	True Anomaly	16
3.8	Hohmann Transfer Diagram	17
3.9	Hohmann Transfer	19
3.10	The behavior of the magnitudes of the primer vector	19
3.11	Relative Motion Trajectories	28
3.12	Orbital Inclination	29
3.13	Ground track of constellation	30
3.14	Simulation	30
4.1	CMOS Image Sensor vs Charge Coupled Device	32
4.2	Micro-controllers	32
4.3	TOSHIBA TCM8230	33
5.1	Hierarchy of Electrical Power Subsystem (Reference: Space mission Design and Analysis , Wiley J Larson, James R Wertz)	36
5.2	Power consumption for each Femto satellite	39

5.3	Solar Panel Selection (Reference: Space mission Design and Analysis , Wiley J Larson, James R Wertz)	40
5.4	Lithium-Ion Coin Battery	44
5.5	Gallium Arsenide Solar Panel	45
5.6	Power consumption for HUB	47
5.7	Solar Panel Selection (Reference: Space mission Design and Analysis, Wiley J Larson, James R Wertz)	49
5.8	Lithium-Ion Battery	52
5.9	Gallium Arsenide Solar Panel	53
5.10	Xl6009 DC - DC voltage converter	54
5.11	OKR-T/3 series DC - DC voltage converter	55
5.12	OPR5910 photodiode based sun sensor	57
5.13	Xtrinsic MAG3110 3-axis digital magnetometer	58
5.14	ITG 3701 3-axis gyroscope	59
5.15	Ferrite core and air core magnetorquers	61
5.16	Basic flow diagram of ADCS	62
5.17	OPR5925 quadrature photodiode and SLCD-61N8 photodiode	64
5.18	Vector Nav VN-100 iIMU	65
5.19	Satbus MTQ M3x magnetorquer and RS-100 reaction wheel	66
5.20	GPS200 outer dimensions (mm)	68
5.21	GPS200 specifications	69
5.22	GPS200	69
5.23	GPS data flow diagram	69
5.24	GPS flow chart	70
5.25	SGR-05P Performance properties	71
5.26	SGR-05P Physical characteristics	72
5.27	SGR-05P	72
5.28	Flow diagram	72
6.1	CC1101 transceiver	76
6.2	CC2500 transceiver	77
7.1	Toshiba TCM8230 CMOS imaging sensor	80
7.2	Toshiba TCM8230 CMOS imaging sensor	81
7.3	ITG-3701 Gyro	81
7.4	Dimensions of ITG-3701 Gyro	81
7.5	MSP432 microcontroller	82

7.6 Dimensions of MSP432 microcontroller	82
7.7 GNSS-200 SERIES NAVIGATION RECEIVER	82
7.8 Dimensions of GNSS-200 SERIES NAVIGATION RECEIVER	83
7.9 Magnetometer- Xtrinsic MAG3110	83
7.10 Dimensions of Magnetometer- Xtrinsic MAG3110	83
7.11 Magnetorquer-Rods	84
7.12 Dimensions of Magnetorquer-Rods	84
7.13 Sun sensor- OPR5910	84
7.14 Dimensions of Sun sensor- OP5910	85
7.15 C1101 transceiver	85
7.16 Dimensions of C1101 transceiver	85
7.17 Air core coil	86
7.18 Dimensions of Air core coil	86
7.19 Driver circuit	86
7.20 Dimensions of Driver circuit	87
7.21 Li-ion battery-RJD3048ST1	87
7.22 Dimensions of Li-ion battery-RJD3048ST1	87
7.23 Gallium Arsenide Solar Panel	88
7.24 Dimensions of Gallium Arsenide Solar Panel	88
7.25 PCB	88
7.26 Dimensions of PCB	89
7.27 Final design 1	89
7.28 Final design 2	89
7.29 Final design 3	90
7.30 Dimensions of Final design	90
7.31 Mass and volume budget for the femto satellite	90
8.1 Spring	97
8.2 Spring Mechanism	97
8.3 Item Specification	98
8.4 Solar panel deployment circuit	98
8.5 Hub Design with solar panels	99
8.6 Hub Design without Solar Panels	100
8.7 Magnetic Torquers	100
8.8 Magnetometer	101
8.9 Dimensions of 6U structure	103
8.10 Steps involved in Dynamical Analysis	104

8.11	Modal Analysis	104
8.12	Random Vibration Profile	105
8.13	Magnetic field lines from a single magnetic torquer shown moving along central axis and ‘spilling over’ to the sides at the top	106
8.14	Magnetic B field of a magnetic torquer modeled as a solenoid	106
8.15	Multiphysics numerical simulation of a single magnetic torquer in free space	106
8.16	Error of numerical computation when compared to analytical solution	107
8.17	B field values for a single magnetic torquer versus the radial distance away from the central axis of the magnetic torquer.	107
9.1	Propulsion Unit for CubeSats (PUC) Mounted on Cubsat structure	110
9.2	Dimensions of Propulsion Unit for CubeSats (PUC) - 0.14U	110
9.3	Interface Diagram	111

List of Tables

3.1	Basic orbital parameters and orbit elements Calculations for Hub satellite	13
3.2	Ground station specification	14
3.3	Ground station specification	14
5.1	Power Required by all the subsystems for Femto-Satellite.	38
5.2	Types of Power sources used in Previous Missions	42
5.3	Power source specifications	43
5.4	Specifications: Lithium-Ion Coin Battery	44
5.5	Specifications: Gallium Arsenide Solar Panel	45
5.6	Power Required by all the subsystems for Hub	46
5.7	Types of Power sources used in Previous Missions	51
5.8	Specifications: Lithium-Ion Battery	53
5.9	Specifications: Gallium Arsenide Solar Panel	53
5.10	Specifications: Xl6009 DC to DC voltage converter	54
5.11	Specifications: Xl6009 DC to DC voltage converter	55
5.12	Magnetorquer parameters - Ferrite core	60
5.13	Magnetorquer parameters - Air-core	60
5.14	Aluminium	61
5.15	PC-47	61
8.1	Nomenclature of Spring	96
8.2	Nomenclature of Spring	97
9.1	Performance matrix	109

Introduction

1.1 | Mission Overview

The primary requirement for a space mission is the mission design. The parameters that were considered during mission design are duration of eclipse, illumination and latitude of the area to be monitored, revisit time, power, and the sequential manoeuvring of the Hub for the successful deployment of the femto-satellites. These influence the orbit that is chosen, the sun-synchronous polar orbit.

The area chosen for monitoring is the Amazon Rain Forest located at $2^{\circ} 9' 47.1816''$ S latitude and $55^{\circ} 7' 35.9328''$ W longitude. The selection of the area is dependent on the proximity of ground stations to the ARF for immediate transfer of captured images. The ground station chosen is the **Kourou Station** in French Guiana, located at $5^{\circ}13'20''$ N latitude and $52^{\circ}46'25''$ W longitude. This ensures a cycle of down-link/up-link between the ground station and the Hub in the same visibility window, which is 11.6 minutes for this mission. In addition to this, the ARF has recorded a 13% increase in forest fires in the first 9 months of 2020. This calls for repeated monitoring to estimate damages and predict trajectories to avoid loss of flora and fauna.

The combination on SSPO, three femto satellites at an orbit of 792km, the Hub at an altitude of 792.5km and a revisit time of 12 hours, serves the requirements provided by the objectives of this mission. The sequence of the mission is as follows:

1. The Hub houses 3 femto satellites, until the desired orbit of 792km.
2. After the successful deployment of the femto satellites, the Hub propels itself to an orbit of 792.5km in order to keep in pace with the femto satellites.

3. Once the Hub and the set of 3 femto satellites take up their respective configuration, they begin working together towards fulfilling their respective objectives.
4. The objective of the femto satellites is to capture images of the affected areas in the ARF.
5. The objective of the Hub is to behave as a communication node between the femto satellites and the Ground station.



Figure 1.1: Schematics of Mission TabSat

1.2 | Aims

1. Femto satellite as a proof of concept-it's survival in space.
2. Reducing the development cycles of femto satellite to make them cost effective.
3. Development of CAD model of femto satellite and the deployer.
4. Inclusion of relay model for communication.
5. Application of femto satellites for remote sensing applications.

1.3 | Objectives

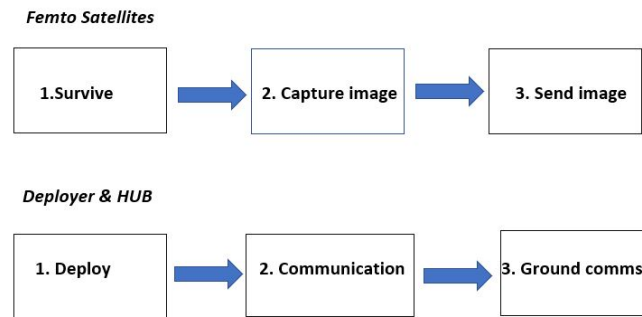


Figure 1.2: Objectives.

1. Femto satellites (TabSat):

- a) **Primary objective:** **Survive-** should be able to send telemetry to the hub, confirm it's position in the configuration.
- b) **Secondary Objective-:** **Imaging-** Click images of forest fires in Amazon Rain Forest- this depends on the power, link and memory budget.
- c) **Tertiary Objective:** **Sending Images-** Sending the captured images to the hub.

2. The HUB and DEPLOYER:

- a) **Primary Objective:** **Deploy-** Deploy the femto satellites in their respective orbit/configuration.
- b) **Secondary Objective:** **Communication-** Communicate with the femto satellites
- c) **Tertiary Objective:** **Ground-** Communicate with the ground

Background & Literature Overview

2.1 | Survey

With the new space revolution scintillating on the horizon of the technological revolution, the advent of small satellites in the field of remote sensing and many other applications such as In-Situ Space weather monitoring, One-Way Satellite inspectors, Upper atmospheric modeling, Terrestrial gamma-ray flash monitoring, which posed a huge challenge to the satellites of conventional size(above 500Kg) (1), now, have become cost efficient and more pronounced(2).

Among the small satellites, femto satellites (weighing just 10-100g) in particular have gained more attention over the past 15 years (3). These are generally operated in clusters under the command of a nearby “mother ship”(which may be another satellite or a dedicated satellite hub). However, recent developments have enabled them to function independently.

In 2011, J. Tristano published the first WikiSat generation, fruit of the N-prize spatial-aerospace competition(4). Wikisat, a typical femto satellite, was housed on Commercial-Off -The-Shelf(COTS) concept due to which there was an inherent flexibility in choosing its peripheral sensors including some optic payloads. This enabled a whole domain of possible research for the femto satellites in remote sensing and observation related space applications.

In 2013, Peru made a breakthrough research in launching femto satellites in the Lower Earth Orbit(LEO), This satellite, designed by the Pontificia Universidad Católica del Perú by the Institute for Radio Astronomy, was called Pocket-PUCP, which transmitted

temperature data (5).

Another well known femto satellite mission, KickSat, launched in 2014, was designed to carry hundreds and thousands of small satellites known as sprites which were essentially microchips. This crowdfunded mission focused on sending radio signals from a large network of sprites that would be released into space to demonstrate the effectiveness of satellite systems in creating a distributed network for low Earth monitoring (6). Even though the sprites burnt during re entry, the KickSat did create a template for future projects utilizing microchip sized femto satellites.

Astrodynamics Subsystem

3.1 | Orbit Selection

For any space mission, resourceful orbit selection is very essential and basic part. Based on the application of the Femto satellite which is disaster monitoring in our case we chose sun-synchronous polar orbit for our mission.

A Sun-synchronous orbit (also called a heliosynchronous orbit) (10) is a nearly polar orbit around a planet, in which the satellite passes over any given point of the planet's surface at the same local mean solar time. More technically, it is an orbit arranged so that it processes through one complete revolution each year, so it always maintains the same relationship with the Sun.

Diagram showing the orientation of a Sun-synchronous orbit (green) at four points in the year:

3.1.1 | Why Sun-Synchronous orbit?

- The orbit is designed in such a way that the angle between the orbital plane and sun remains constant resulting in inconsistent lighting conditions.
- The satellites in this orbit can help in monitoring activities near the poles, unlike other satellites (12).
- The Sun-synchronous orbiting satellites cover the entire globe on regular basis and provide repetitive coverage periodically.

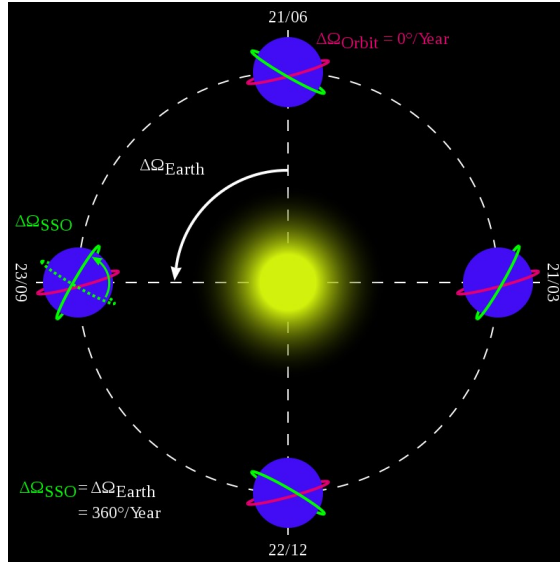


Figure 3.1: Sun-synchronous Polar Orbit (11)

- Satellite passes overall places on earth having the same latitude twice in each orbit at the same local sun time.
- The low altitude of this orbit allows good ground resolution.
- Satellite in SSPO shifts its orbital plane approx. one degree/day to keep pace with the Earth's movement around the Sun.
- Solar panels of the satellite in SSPO always face the sun beneficial for power generation without being shadowed by the Earth.

Special cases of the Sun-synchronous orbit are the noon/midnight orbit (10), where the local mean solar time of passage for equatorial latitudes is around noon or midnight, and the dawn/dusk orbit, where the local mean solar time of passage for equatorial latitudes is around sunrise or sunset so that the satellite rides the terminator between day and night. We decided to go with dawn/dusk orbit since riding the terminator is useful for imaging satellites, as the satellites' solar panels can always see the Sun, without being shadowed by the Earth. The dawn/dusk orbit has been used for Earth observation satellites such as Radarsat-211 which we took as a reference satellite for calculations.

3.2 | Computer Program for Predicting Orbital Events

This section shows a Computer Program for Predicting Orbital Events of Mission TabSat:

```
< Prediction of orbital events for the Mission TabSat >

semimajor axis (kilometers)
(semimajor axis > 0)
7170
orbital eccentricity (non-dimensional)
(0 <= eccentricity < 1)
0.0125

orbital inclination (degrees)

(0 <= inclination <= 180)
98.57

argument of perigee (degrees)
(0 <= argument of perigee <= 360)
0

right ascension of the ascending node (degrees)

(0 <= RAAN <= 360)
0

true anomaly (degrees)
(0 <= true anomaly <= 360)
0

initial calendar date and time

please input the calendar date
(1 <= month <= 12, 1 <= day <= 31, year = all digits!)
```

? 10,08,2020

```
please input the universal time  
(0 <= hours <= 24, 0 <= minutes <= 60, 0 <= seconds <= 60)  
? 0,0,0
```

```
please input the simulation period (min)  
? 100.71
```

algorithm control parameters

```
please input the integration error tolerance (a value of  
1.0e-8 is recommended)  
? 1.0e-8
```

```
please input the root-finding error tolerance  
(a value between 1.0e-4 and 1.0e-6 is recommended)  
? 1.0e-4
```

gravity model inputs

```
please input the degree of the gravity model (zonals)  
(0 <= zonals <= 18)  
? 2
```

```
please input the order of the gravity model (tesseral)  
(0 <= tesseral <= 18)  
? 0
```

orbital perturbations

```
would you like to include solar perturbations (y = yes, n = no)
```

```
? n
```

```
would you like to include lunar perturbations (y = yes, n = no)
```

```
? n
```

```
would you like to include drag perturbations (y = yes, n = no)
```

```
? y
```

```
would you like to include srp perturbations (y = yes, n = no)
```

```
? n
```

```
orbital elements menu
```

```
<1> user input
```

```
<2> data file
```

```
? 1
```

```
please input the semi-major axis (kilometers)
```

```
(semi-major axis > 0)
```

```
? 7170.5
```

```
please input the orbital eccentricity (non-dimensional)
```

```
(0 <= eccentricity < 1)
```

```
? 0.025
```

```
please input the orbital inclination (degrees)
```

```
(0 <= inclination <= 180)
```

```
? 98.57
```

```
please input the argument of perigee (degrees)
```

```
(0 <= argument of perigee <= 360)
? 91.5702
```

```
please input the right ascension of the ascending node (degrees)
```

```
(0 <= raan <= 360)
? 278.9379
```

```
please input the true anomaly (degrees)
```

```
(0 <= true anomaly <= 360)
? 190
```

```
aerodynamic drag inputs
```

```
please input the drag coefficient (non-dimensional)
? 2
```

```
please input the cross-sectional area (square millimeters)
? 76840
```

```
please input the spacecraft mass (kilograms)
? 5.5
```

```
please select the orbital element to predict
```

```
<1> altitude
```

```
<2> latitude
```

```
<3> longitude
```

```
<4> declination
```

```
<5> true anomaly
```

```
<6> argument of latitude
```

<7> flight path angle

<8> orbital speed

<9> right ascension

? 2

please input the geodetic latitude (degrees)

(-90 <= latitude <= +90)

? 52.77

3.3 | The Constellation of Femto satellites and HUB

We have proposed a design for a constellation 5 of three femto satellites which will be deployed in the same orbital plane at an altitude of 7170 km with specific Δt by the deployer. After a successful deployment of all satellite deployer will work as HUB satellite to collect the data from the satellites and relay it to the ground station. HUB satellite will be transferred to its target orbit at an altitude of 7170.5 km using Hohmann Transfer Orbit (13).

Orbit type	Sun-Synchronous polar orbit
Altitude	7170 km
Inclination	98.57
Eccentricity	0.0125
Semi-major	axis 7170 km
Argument of perigee(deg)	Undefined
Long. of ascending node(deg)	Undefined
True anomaly (deg)	Undefined
Orbital period	100.702 min
No. of orbit per day	14.2996
Orbital velocity	7.4560 km/sec
Revisit	12 hrs.
Repeat cycle	3 Days,8hrs,9min,35sec / 48orbit
Epoch (reference time)	29/sep/2020 21:07:58 UTC

Orbit type	Sun-Synchronous polar orbit
Altitude	7170.5km
Inclination	98.57
Eccentricity	0.025
Semi-major axis	7170.5km
Argument of perigee(deg)	91.5702
Long. of ascending node(deg)	278.9379
True anomaly (deg)	190
Orbital period	100.71
No. of orbit per day	14.2984
Orbital velocity	7.4557 km/sec

Table 3.1: Basic orbital parameters and orbit elements Calculations for Hub satellite

Ground station for data relay	Kourou station, French Guiana, Guiana Space Centre, South America
Coordinates	5°13'20"N 52°46'25"W
Revisit	12 hrs.
Details of a ground station	The station hosts a 15-m dish antenna that transmits and receives signals in S- and X-band wavelengths

Table 3.2: Ground station specification

Targeted Area	Amazon forest
Coordinates	3°27'55.1"S, 62°12'57.2"W
Revisit	12 hrs
Radius	1500 km
Area	7068583.47 Sq.km

Table 3.3: Ground station specification

3.4 | Data Visualization of Orbital Parameters

A series of data visualisation results for the 6 main parameters in a given simulation time of 1410 min is proposed as below:

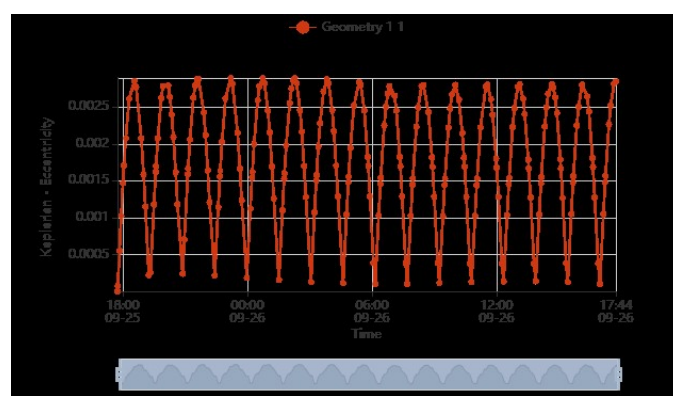


Figure 3.2: Eccentricity



Figure 3.3: Inclination

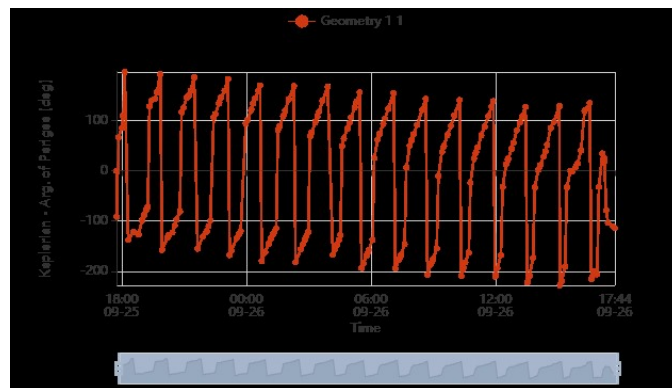


Figure 3.4: Argument of Perigee



Figure 3.5: Longitude of Ascending Node

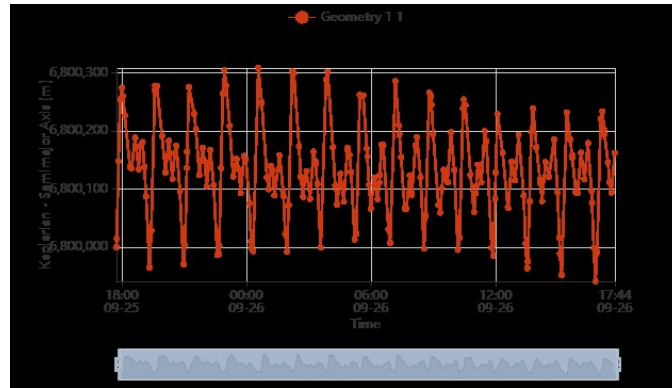


Figure 3.6: Semi-major axis

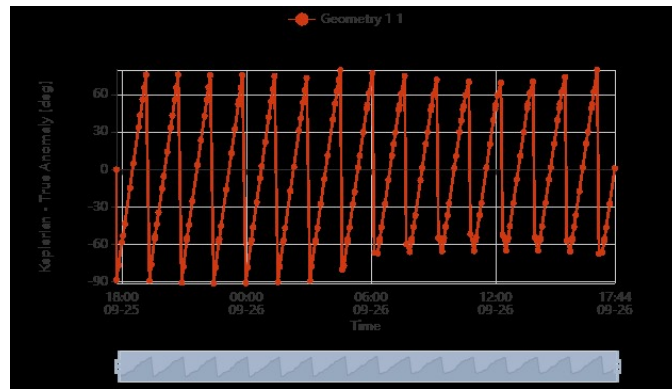


Figure 3.7: Truly Anomaly

3.5 | Calculations of Hohmann Orbit Transfer

(13)

In orbital mechanics, the Hohmann transfer orbit is an elliptical orbit used to transfer between two circular orbits of different radii around a central body in the same plane. To raise orbit from parking orbit (Femtosat deployment orbit (15)) to target orbit with less fuel consumption Hohmann transfer orbit can be used. Following calculation shows total change in velocity required for HUB satellite to achieve targeted orbit.

In the below diagram, you see a good depiction of a Hohmann transfer. In part 1 (the green orbit), the satellite is in a "parking orbit" which is a Low Earth Orbit that is achieved shortly after launch. In part 2 (the yellow orbit), a maneuver is performed, increasing the velocity of the satellite until its orbit is an ellipse with an apogee at the target orbit's semi-major axis. This part is called the transfer trajectory. Once the space-

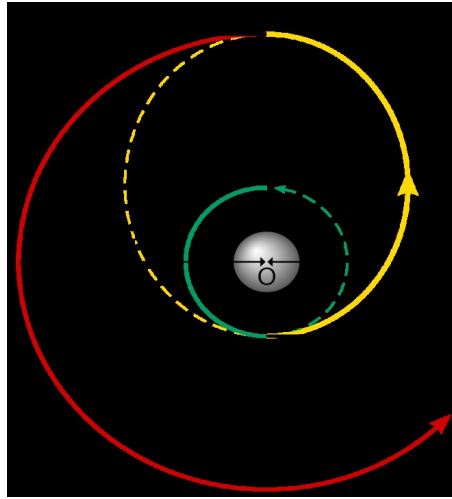


Figure 3.8: Hohmann Transfer Diagram

craft reaches the apoapsis of that trajectory, it performs an orbital insertion burn (16). This increases the velocity, matching the orbit to its target circular orbit.

Every calculation will be based around the Vis-Viva Equation:

$$v = \sqrt{\mu \left(\frac{2}{r} - \frac{1}{a} \right)}$$

v = velocity

μ = Standard Gravitational Parameter of the Central Body (398600.442 km³/s² for Earth)

r = Radius from Earth

a = Orbit Semi-Major Axis

The first step we must take is finding the velocity of the parking orbit. If we use the variables $r = 7170\text{km}$, $a = 7170\text{km}$, and the standard gravitational parameter of Earth, we can find v.

$$v_{\text{park}} = 7.4560\text{km/s}$$

Next, we must find the orbital characteristics of the transfer orbit (17). First, we must find the semi-major axis of the transfer orbit. To do this, we can take the average of the semi-major axes of the target orbit and the parking orbit.

$$a = \frac{a_{\text{Target}} + a_{\text{Parking}}}{2} = \frac{(7170.5 + 7170)}{2} = 7170.25\text{km}$$

Now, we can find the velocity at periapsis of this transfer orbit. In this case $r = 7170km$, and $a = 7170.25km$. We plug these into the Vis-Viva equation to get:

$$v_{\text{transfer peri}} = 7.4562 \text{ km/s}$$

Then, we can calculate the Δv of the first maneuver:

$$\Delta v1 = v_{\text{transfer peri}} - v_{\text{park}} = 0.2 \text{ m/s}$$

This first burn will put our Spacecraft into its transfer orbit. Next, we need to calculate the speed at the transfer orbit's apoapsis. For this calculation, $r = 7170.5km$, and $a = 7170.25km$. We plug these into the Vis-Viva equation to get:

$$v_{\text{transfer apo}} = 7.4556 \text{ km/s}$$

Now, we must calculate the velocity of the target orbit. For the variables, $r = 7170.5km$, and $a = 7170.5km$. We plug these into the Vis-Viva equation to get:

$$v_{\text{target}} = 7.4558 \text{ km/s}$$

Now, we can calculate the Δv for the insertion burn, and finally the total Δv :

$$\Delta v2 = v_{\text{target}} - v_{\text{transfer apo}} = 0.2 \text{ m/s}$$

$$\Sigma \Delta v = \Delta v1 + \Delta v2 = 0.4 \text{ m/s}$$

3.6 | Data Visualization of Gravity Perturbed Hohmann Orbit Transfer

This section shows the Data Visualization for Analysis of Gravity Perturbed (19) Hohmann Orbit Transfer for Femoyer Mission: (23; 26)]

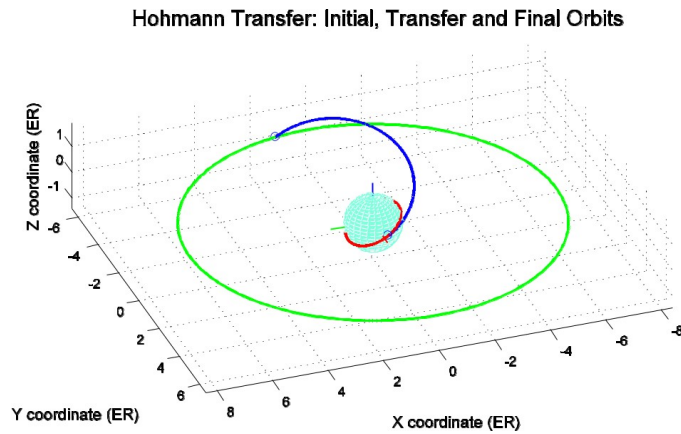


Figure 3.9: Hohmann Transfer

The following two graphic images illustrate the behavior of the magnitudes of the primer vector and its derivative for Gravity Perturbed Hohmann Orbit Transfer.

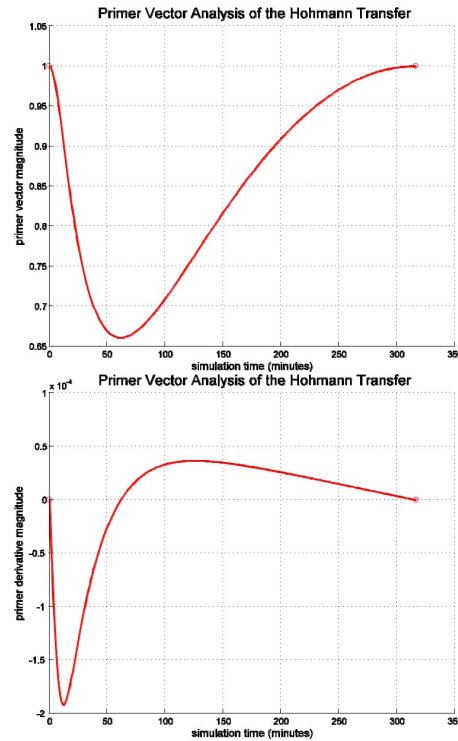


Figure 3.10: The behavior of the magnitudes of the primer vector

3.7 | Computer Program for Solving Gravity Perturbed Trajectory Problem and for Targeting the Orbit

This computer Program can be used to solve the gravity perturbed Hohmann transfer between coplanar and non-coplanar circular Earth orbits. The algorithm starts with a two-body Hohmann transfer initial guess. We also provide a program for targeting the Orbit of Femoyer Mission.

```
< Gravity model and Orbit Targeting for Femoyer Mission>

function [ccoef, scoef] = readgm(fname)

read gravity model data file

input

fname = name of gravity data file

output

ccoef, scoef = gravity model coefficients

data file format (space delimited ascii)

read the data file

gdata = dlmread(fname);

nrows = size(gdata, 1);

initialize coefficients

idim = gdata(nrows, 1) + 1; ccoef = zeros(idim, idim); scoef = zeros(idim, idim);

create gravity model coefficients for n = 1:nrows
```

```
i = gdata(n, 1);

j = gdata(n, 2);

ccoef(i + 1, j + 1) = gdata(n, 3);

scoef(i + 1, j + 1) = gdata(n, 4);

End

% initial guess for components of initial delta-v

xg(1) = vti(1) - vi(1);
xg(2) = vti(2) - vi(2);
xg(3) = vti(3) - vi(3);

% initial guess for components of final delta-v

xg(4) = vf(1) - vtf(1);
xg(5) = vf(2) - vtf(2);
xg(6) = vf(3) - vtf(3);

xg = xg';

define lower and upper bounds for components of delta-v vectors (kilometers/second)

dvm = norm(xg(1:3));

for i = 1:1:3

xlwr(i) = xg(i) - 0.01; xupr(i) = xg(i) + 0.01;
end

dvm = norm(xg(4:6)); for i = 4:1:6

xlwr(i) = xg(i) - 0.01; xupr(i) = xg(i) + 0.01;
```

```
end

xlwr = xlwr'; xupr = xupr';
bounds on objective function

flow(1) = 0.0d0;

fupp(1) = +Inf;

flow(2) = 0.0d0;
fupp(2) = 0.0d0;

flow(3) = 0.0d0;
fupp(3) = 0.0d0;

flow(4) = 0.0d0;
fupp(4) = 0.0d0;

flow(5) = 0.0d0;
fupp(5) = 0.0d0;

if (itarget <= 1.0d-8)

% sun synchronous orbit constraint

flow(6) = 0.0d0;
fupp(6) = 0.0d0;

end

flow = flow';
fupp = fupp';

read SNOPT specs file snspe('snopt
_specs.txt');
```

```
snscreen on;

[x, f, inform, xmul, fmul] = snopt(xg, xlwr, xupr, flow, fupp, 'tpbvp');

function ydot = ceqm1 (t, y)
first order form of Cowell's equations of orbital motion

version for ode45

input

t = current simulation time
y = current eci state vector

output

ydot = eci acceleration vector

% compute circular gravity perturbations

aggrav = gravity(t, y);

% total acceleration vector

ydot = [ y(4)
y(5)
y(6)
aggrav(1)
aggrav(2)
aggrav(3)] ;

% set up options for ode45
```

```
options = odeset('RelTol', 1.0e-12, 'AbsTol', 1.0e-12, 'Events', @nc_event);

solve for nodal crossing condition rwrk = xi(1:3);

vwrk = xi(4:6);

maximum search duration = 102

[t, ysol, tevent, yevent, ie] = ode45(@ceqm1, [0 tend], [rwrk vwrk], options);

function [value, isterminal, direction] = nc_event(t, y)

% nodal crossing event function required by femoyer mission

z-component of the unit position vector value = y(3) / norm(y(1:3)); isterminal
= 1;
direction = -1;
% enforce semiparameter and circular orbit constraints (p, f = g = 0) f(2) =
mee_final(1) - mee_target(1);

f(3) = mee_final(2) - mee_target(2);

f(4) = mee_final(3) - mee_target(3);

enforce mission orbit inclination constraint(s) if (itarget <= 1.0d-8)

Sun synchronous orbit (h = k = 0)

f(5) = mee_final(4);

f(6) = mee_final(5);

else

% sun synchronous mission orbit ( $h^2 + k^2 = 0$ )
```

$f(5) = (mee_final(4)^2 + mee_final(5)^2) - (mee_target(4)^2 + ... mee_target(5)^2);$

End

3.8 | Computer Program for Analysis of Relative Motion Trajectories between two Femto satellites

Following is a Computer Program for Analysis of Relative Motion Trajectories between two Femto satellites:

INPUT

graphics display of relative motion

relative motion menu

<1> user input of initial conditions

<2> calculate and display synchronous orbit <3> calculate and display rendezvous orbit selection (1, 2 or 3)

? 1

please input the altitude of the target satellite (kilometers)

? 1710

please input the initial x-position of the chaser satellite (kilometers)

? 10

please input the initial y-position of the chaser satellite (kilometers)

? 10

```
please input delta-vx of the chaser satellite (meters/second)
? -3
```

```
please input delta-vy of the chaser satellite (meters/second)
? 5
simulation time menu
```

```
<1> user input of simulation time
```

```
<2> simulate for one orbital period
```

```
selection (1 or 2)
```

```
? 2
```

```
please input the plot step size (minutes)
? 1
```

```
OUTPUT
```

```
graphics display of relative motion
```

```
relative motion menu
```

```
<1> user input of initial conditions
```

```
<2> calculate and display synchronous orbit
```

```
<3> calculate and display rendezvous orbit
```

```
selection (1, 2 or 3)
```

```
? 2
```

```
please input the altitude of the target satellite (kilometers)
? 1710
```

```
please input the initial x-position of the chaser satellite (kilometers)
```

```
? 10
```

```
please input the initial y-position of the chaser satellite (kilometers)
```

```
? 10
```

```
the orbital period is 100.71 minutes
```

```
simulation time menu
```

```
<1> user input of simulation time
```

```
<2> simulate for one orbital period
```

```
selection (1 or 2)
```

```
? 2
```

```
please input the plot step size (minutes)
```

```
? 1
```

3.9 | Data Visualization of Relative Motion Trajectories between two Femto satellites

This section shows the data visualization of a relative motion between two femtosatellites: (22; 27)

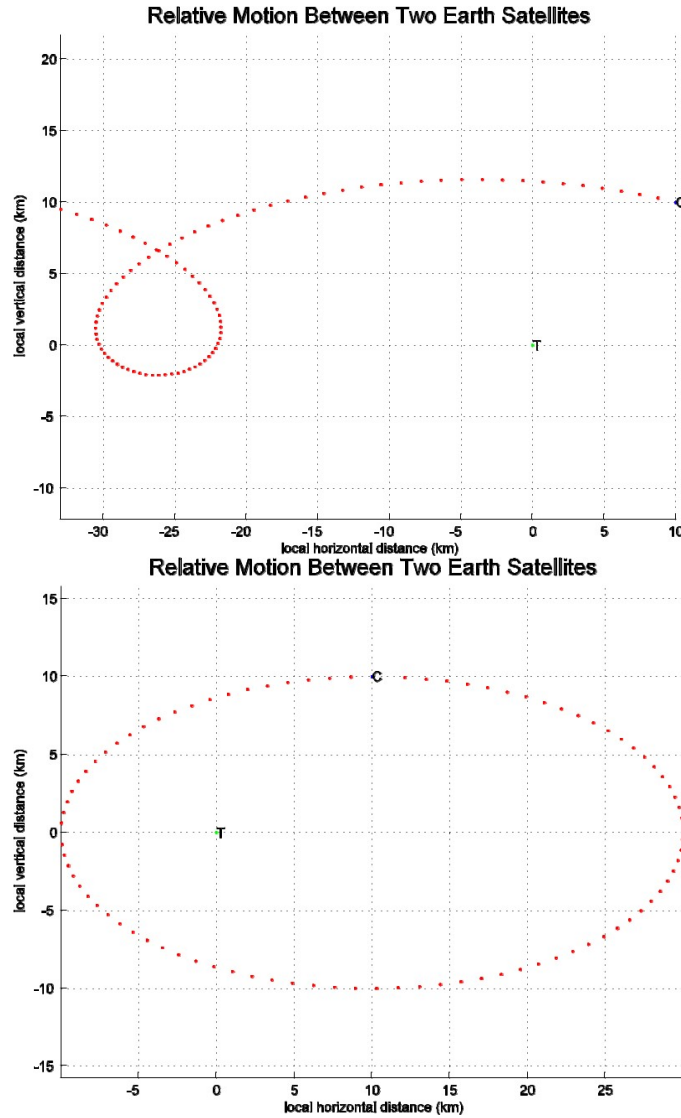


Figure 3.11: Relative Motion Trajectories

3.10 | Maximization of Orbital Inclination

This section shows the graphics for an aero-assist trajectory that maximizes the orbital inclination change. Femoyer-Hub has been given a constant inclination of 98.57 during all stages of the mission. The speed at atmospheric exit is constrained to be ≥ 4.572 km/sec.

The following are plots of the important trajectory parameters for the Femoyer Mission: (24).

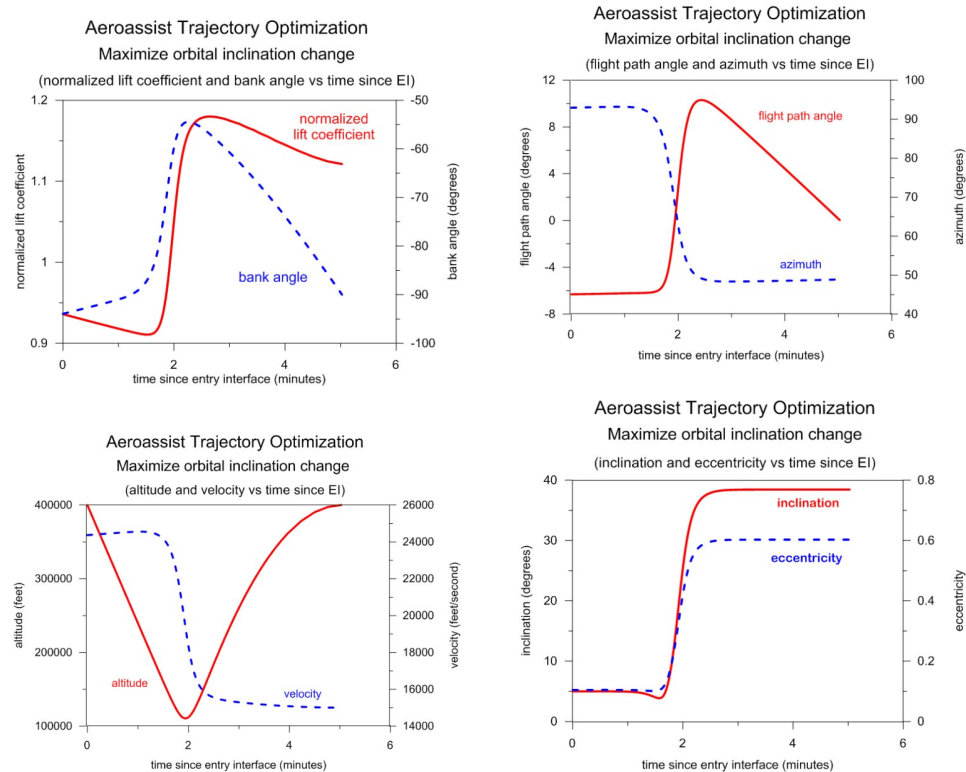


Figure 3.12: Orbital Inclination

3.11 | Orbit Design and Simulation

Femoyer Mission Orbit has been designed and Simulated using STK and Savoir Software.



Figure 3.13: Ground track of constellation

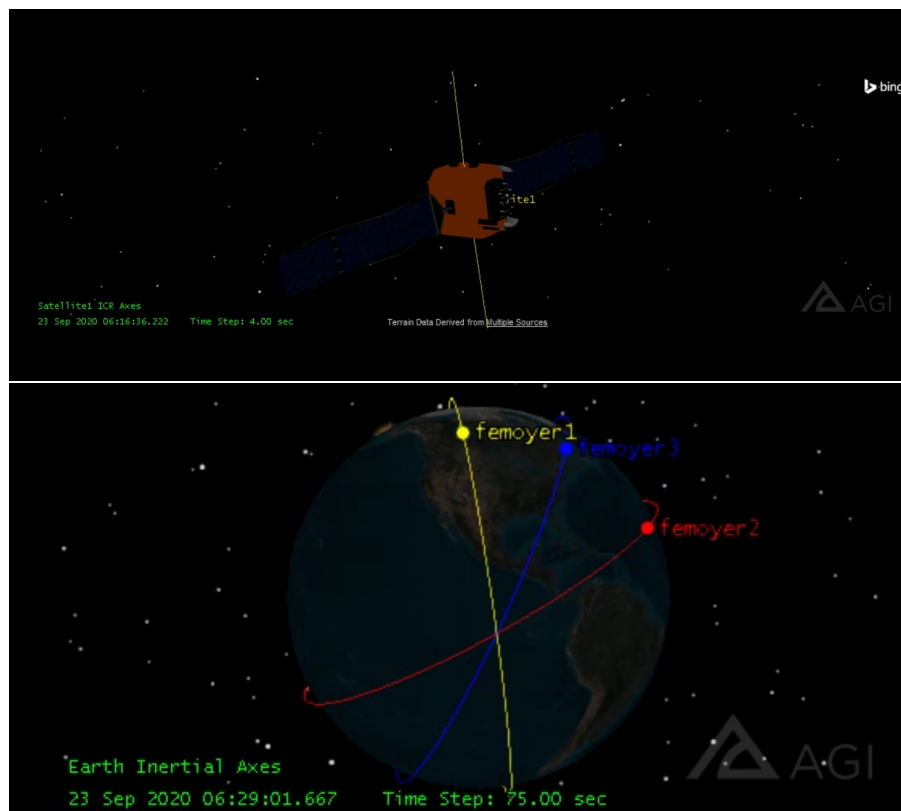


Figure 3.14: Simulation

Payload Subsystem

4.1 | Workflow

The entire workflow of the payload subsystem was broadly divided into:

- Analyzing the constraints faced by the femto-satellites in the orbit
- In depth analysis of the working of the CMOS sensor
- Sending the captured images to the ground station for image processing.
- Analyzing the surface of the earth for remote sensing applications.

Conducted Comparative study of the following:

Image Sensor

Finalized the CMOS image sensor due to its high compatibility with the femto-satellites

- All components are integrated into a single chip
- High response capability
- Lower operating voltage reducing overall load requirements
- Dynamic operating temperature range

Micro-controllers

Compared different microcontrollers considering various factors.

Major factors which were found to play a major role in determining the compatibility with femto-satellites:

1. Memory requirements (decided to go with flash memory)
2. Operating voltage
3. Number of GPIO pins
4. Operating temperature

Property	Charge-Coupled Device	CMOS Image Sensor
Operating Voltage	12V-15V	2.8V-5V
Response Capability	Nil	High
Image Capture Time	Similar	Similar
Size Feasibility	Requires external additional components	Integrates all components into a single chip, highly suitable for a femtosat
Dynamic Range	CCD does not integrate the digitization of the signal into the sensor so additional components are used to carry out this process to reduce noise	Very low-requires the use of complex filters to reduce noise
Blooming	Highly sensitive	Not sensitive
Windowing	not possible	possible
Operating Temperature	Requires refrigeration techniques as temperature doubles every 7 C.	-40C-115C

Figure 4.1: CMOS Image Sensor vs Charge Coupled Device

Microcontrollers			
Microcontrollers	ATmega 128	CC430F6137	ARM Cortex M4 family
Parameter			
Memory			
Flash	168 KByte	32 KByte	1 MByte
EEPROM	512 Byte	NA	{4KByte}
RAM	1KByte	4 KByte	192+4 KByte
OTP Memory	NA	NA	512 Bytes
ADC	10 bits	12 bits	2x12 bit
Pins	32	48	64 100 144 176
GPIO	23	30	51 72 82 114 140
Operating Voltage	2.7 to 5.5 V	1.8 to 3.6 V	1.8 to 3.6 V
Operating Temperature (degree Celsius)	-40 to 150	-40 to 85	-40 to 105
Dimensions	7x7 mm	7x7 mm 9x9 mm	10x10 mm

Figure 4.2: Micro-controllers

In depth analysis of TOSHIBA TCM8230

Toshiba TCM8230		
Camera	Photo diode I/O	2.5V
	ADC	1.5V
Temperature		
	Storage	-30 to 85 deg C
	Operational temperature	-20 to 60 deg C
	Size	6X6X4.5mm
	weight	0.18g
Lens	Pixel numbers	698(h)X502(v)
Field of view		
	Horizontal	57.4 deg
	Vertical	44.5 deg
	Diagonal	69.1 deg
Resolution (h=250km)		
	Pixel size	344 m
	Area	240X173km
	Structure	Double lens
Optional telephoto lens	Field of view	8 deg
	Map resolution (h=250 km)	
	Pixel size	50 meters
	Cylinder size	dia= 21.4mm h=70mm
	Cylinder weight	0.82g

Figure 4.3: TOSHIBA TCM8230

- Understood that the field of view of the camera would play a major role in determining the number of femto-satellites in each cluster.
- Analyzed the lens properties in depth to get a clear idea about its resolution and field of view and the number of pixels of the image it can capture.
- The maximum view along all possible directions was also taken into consideration.

MSP432 Microcontroller:

- The MSP432 Microcontrollers by Texas Instruments are efficient ultra-low-power mixed-signal MCUs. With a rich set of analog, timing, and communications peripherals, they cater to a large number of application scenarios.
- This family of MCUs is the heart of the electronics subsystem of our femto-satellite mission which is used as a micro-controller for both the satellite and the deployer.
- The MSP 432E401Y uses ARM cortex m4 as core 32 bit with 90 GPIO pins and operating frequency of 120Mhz.
- It has a dimension of 10*10mm - 12*12mm which is highly compatible for a small satellite mission.
- It has an operating temperature of -40 to 105 C.
- Other specifications: 1024 KB flash memory, 256 KB RAM, 6KB EEPROM, clock - 120-MHz.
- Its high capability of flash memory would facilitate image capturing and storage for image processing.
- It is also highly compatible with the CMOS image sensor. Some of its important features are:
 - 48MHz ARM Cortex-M4 with FPU
 - Wide voltage range
 - Simultaneous Flash read/write
 - 128-bit Flash buffer and pre-fetch
 - Selectable RAM retention
 - 64KB RAM
 - 1MSPS ADC14
 - 8-channel DMA
 - Memory protection unit
 - Integrated LDO and DC/DC
 - Tuneable DCO
 - Peripheral and SRAM memory bit-band

- 20mA high drive I/Os
- 32-bit timer
- JTAG security and advanced IP protection

Area Covered by imaging sensor: At orbits closer to 90°inclination

$$S_{\text{Pixel}} = \frac{h \sin(\frac{\text{FOV}}{2})}{\text{Pixelsize}/2}$$

Horizontal (FOV = 57.4°) = 760.7km

Vertical (FOV = 44.5°) = 599.7km

Electrical Subsystem

5.1 | Electrical Power Subsystem

Electrical Power system (EPS) design in any satellite mission plays a crucial role in the survivability of the satellite. Its major function includes generation, storage, distribution and control of electrical power required for the entire mission. It also influences a large number of the other systems like payload, communication and electronics etc (28).The major peak and average loads need to be identified.

The electrical power system of satellite mission comprises of 4 subsystems as shown in the Figure 1.

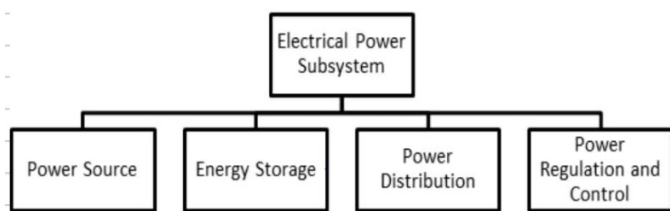


Figure 5.1: Hierarchy of Electrical Power Subsystem (Reference: Space mission Design and Analysis , Wiley J Larson, James R Wertz)

It is very important to calculate the above parameters for a reliable power subsystem design. For the designing of EPS system for our Femto-satellite mission a large literature study was carried out and a general idea of the commonly used system design was understood.

5.1.1 | Literature Survey

In order to develop a better idea about the EPS system design, functioning and design procedure, many papers with similar mission objectives for Femto-satellites were referred and understood. Several researchers have previously worked on a similar mission. Some of supporting evidence for the EPS includes a literature survey from the below works:

To understand how the design of an EPS system in a satellite mission works, the book “Space Mission Design and Analysis” by Wertz and Larson was referred. It gave a general idea about the procedure to carry out the power budget (28). The stardust Femto-satellite mission utilized Gallium Arsenide panels to utilize solar energy as its major source of power. This also gave us a frame work on what could be the possible options for power system (29).

In the paper “Design of a COTS Femto-satellite and Mission” by G. McVittie and K. Kumar give an idea on the approach to Commercial Off the shelf components in Femto-satellite. This helped us to select components that were readily available in the market (30). Also the PCBSAT mission set a framework on the detailed EPS system for the Femto-satellite that was very helpful in understanding the initial constraints (31). The paper on “Study of Current Femto-Satellite Approches” by N. Tahri, C. Hamrouni, and A. M. Alimi was a wealth of knowledge to us on the current Femto-satellite missions and its system design. Some other referred literature work for the EPS was the Kicksat, Wikisat and Pocket-PUCP mission (32).

5.2 | Objectives

The major objectives of the electrical subsystem include:

- Providing intermittent source of power to all the components at a required point of time
- To distribute power in a regulated manner
- To prevent faults and failures in the electrical power system
- To satisfy the power requirements of all the subsystem

5.3 | Power Budget: Femto Satellite

5.3.1 | Power required by all subsystems

The power required by all the subsystems for the Femto-satellite design was collected and summarized as follows:

Table 5.1: Power Required by all the subsystems for Femto-Satellite.

Component	No. of Components to be used	Low Voltage V	Average Voltage V	Peak Voltage V	Current mA	Power consumed based on average voltage mW	Power consumed based on peak voltage mW
MSP 432E401Y; f= 120MHz	1	2.97	3.3	3.63	0.642	2.1186	2.33046
Xtrinsic MAG3110 Three-Axis, Digital Magnetometer	1	1.95	2.4	3.6	NA	2.16	3.24
ITG-3701 3-axis gyro	1	1.71	4	3.6	5	20	18
MT01.1 magnetorquer	3	NA	2.5	5	59	147.5	180
Toshiba TCM8230 CMOS camera	1	1.4	2.2	3	40	88	120
GNSS-200 SERIES NAVIGATION RECEIVER	1	NA	NA	3.6	150	75	150
CC1101 Transceiver	1	1.8	NA	3.6	100	5	10

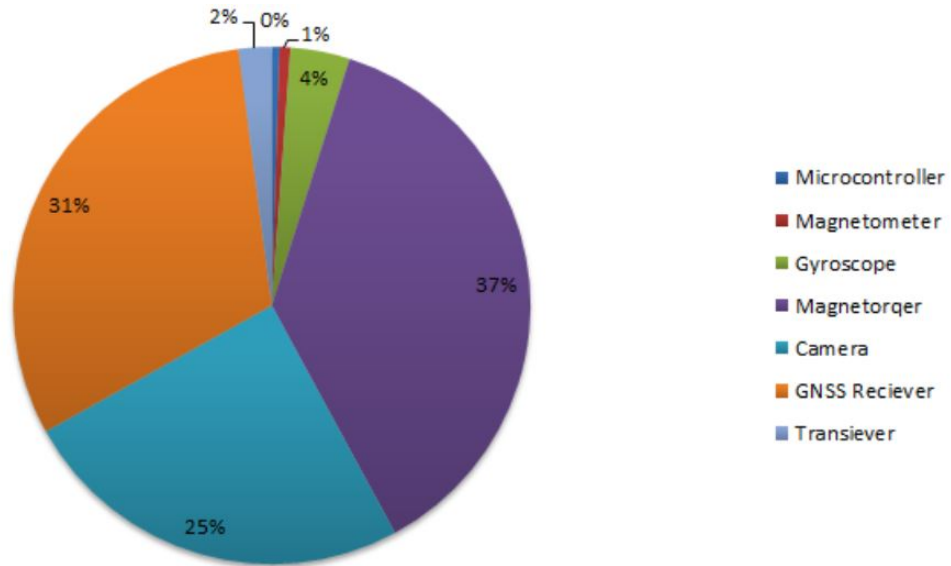


Figure 5.2: Power consumption for each Femto satellite

Based on the sum of the power requirement of all the subsystems, a rough power requirement with a buffer of 20% was considered to be 500mW based on the peak voltage. In a practical scenario, not all the components will be operating at the same time.

5.3.2 | Power Generation

Generating Power in space environment has always been a complex concept of research. One of the major sources of energy that can be utilized for generating power in space , is the Solar Energy. Based on our mission objectives, the orbit selected was sun synchronous orbit, which eliminated the eclipse occurrence. The major source of power generation was considered to be solar energy. This energy is generated using solar panels mounted on the satellite body. In order to select the solar panels for this mission, the amount of power required to be produced by the solar panel needs to be calculated as a part of the power budget and a panel that satisfies our mission objectives is to be selected (28).

Amount of Power to be produced by the Solar Array P_{sa}

The amount of power needed to be generated by the panels was calculated using the equations below to be 1.5 W.

$$P_e = P_d = 500mW \text{ (Based on Peak Voltage from Table 1)}$$

$$T_e = T_d = 100 \text{ min}(\text{orbital period})$$

Assuming Peak Power Tracking Regulation Scheme

$$X_e = 0.6X_d = 0.8(\text{Efficiencies of the power distribution Path})$$

$$P_{sa} = \frac{\frac{P_e T_e}{X_e} + \frac{P_d T_d}{X_d}}{T_d} = 1.5W$$

Where,

P_{sa} = Amount of power to be produced by the Solar Array

P_e & P_d = Spacecraft power requirements (Excluding regulation and battery charging losses)

T_e & T_d = Lengths of the period per orbit

X_e & X_d = Efficiencies of the power distribution paths

Ideal Power Production

Estimating Solar Cells power output P_o , with the sun normal to the surface of the cells

In order to determine the power output that can be produced by a solar cell, here the gallium arsenide solar panel is selected. This panel was selected due to the various advantages that it offers for our mission. It has a much better efficiency in comparison to silicon solar panel. But it is 3 times much costlier than the traditional silicon solar panel (28). In this step, to identify the correct type of panel to suit our mission the following table was considered as a source of reference.

TABLE 11-35. Performance Comparison for Photovoltaic Solar Cells. Note that the stated efficiencies are for single solar cells, not solar arrays.

Cell Type	Silicon	Thin Sheet Amorphous Si	Gallium Arsenide	Indium Phosphide	Multijunction GaInP/GaAs
Planar cell theoretical efficiency	20.8%	12.0%	23.5%	22.6%	25.8%
Achieved efficiency: Production Best laboratory	14.8% 20.8%	5.0% 10%	18.5% 21.8%	18% 19.9%	22.0% 25.7%
Equivalent time in geosynchronous orbit for 15% degradation – 1 MeV electrons – 10 MeV protons	10 yr 4 yr	10 yr 4 yr	33 yr 6 yr	155 yr 89 yr	33 yr 6 yr

Figure 5.3: Solar Panel Selection (Reference: Space mission Design and Analysis , Wiley J Larson, James R Wertz)

It was found out that the achieved performance efficiency for gallium arsenide panel was found to be 18.5% (28). Using this information the idea cell power output per unit area can be calculated as follows. (Efficiency of 18.5%)

$$\text{Solar Constant} = 1,367 \text{ W/m}^2$$

$$P_o = 0.185 * 1,367 = 253 \text{ W/m}^2$$

Realistic Power Production Realistic power production capability of the manufactured solar array is the most important parameter to be calculated. In real-time there are various factors that affect the actual power produced and is far different from the idealistic case. Here comes the concept of inherent degradation, I_d . The various factors that account for inherent degradation is due to design and assembly, temperature of array etc (28).

Beginning of Life Power Production Capability P_{bol} Radiation damage severely reduces a solar array's output voltage and current. Life degradation, LD occurs because of thermal cycling in and out of eclipses, micro-meteoroid strikes, plume impingement from thrusters etc.

$$I_d = 0.77$$

At sun synchronous orbit, $\theta = 0$ There is a code mistake in the above two formulae

Where,

θ = Sun Incidence Angle

$\cos \theta$ = Cosine loss

Maximum power will be produced when the Sun's rays are perpendicular to the solar array's surface.

End of Life Power Production Capability P_{eol}

Radiation damage severely reduces a solar array's output voltage and current. Life degradation, L_d occurs because of thermal cycling in and out of eclipses, micrometeoroid strikes, plume impingement from thrusters etc. For gallium-arsenide cells in LEO, the degradation is about 2.75% per year, of which radiation causes 1.5% per year (28).

The actual lifetime degradation can be estimated using

$$L_d = (1 - \text{degradation/yr})^{\text{satellitelife}} \quad (\text{ActualLifetimeDegradation})$$

$$L_d = (1 - 0.0275)^1 = 0.9725$$

The array's performance per unit area

$$P_{eol} = P_{bol} L_d$$

$$P_{eol} = 189.45 \text{ W/m}^2$$

Area of the solar Array required

The area required to support the power requirement of the subsystem is

$$A_{sa} = \frac{P_{sa}}{P_{eol}} = \frac{1.5}{189.45} = 79 \text{ cm}^2$$

Mass of the solar Array required

The mass of the required solar panel can be calculated as follows:

$$M_{sa} = 0.04 P_{sa} = 0.04 * 1.5 = 0.06 \text{ kg} = 60 \text{ gm}$$

5.3.3 | Power Storage

In a few Femto-satellite missions the most common option of power source used is coin battery. For considering various possible options, we referred to a large number of possible options considering the previous missions. The table below provides a general idea of the various power sources that were used in previous relevant Femto-Satellite missions.

Mission Name	Power Type
Pocket PUCP	Solar Cell +Lithium Polymer Battery
Suncube 3TJ	Solar cell + Lion Battery
Ryefemsat	Solar Array +Lithium Polymer Battery
Wikisat	Coin Battery and Solar cells
SWIFT	Photovoltaic cells major source
Stardust	Solar Array Chip

Table 5.2: Types of Power sources used in Previous Missions

For our mission we considered a secondary battery that was rechargeable using solar energy for power. Lithium ion battery was selected, because with 65% volume advantage and a 50% mass advantage (28). The Depth of Discharge (DOD) for Lithium-Ion Battery is assumed to be 30%. After developing a general idea, the calculation to select the battery was carried out as follows:

Battery Selected	Lithium Ion Battery
Nominal Voltage	upto 3.7 Vdc
No of Batteries N	
Transmission Efficiency Between the battery and Load	n=0.9
Depth of Discharge(DOD)	0.3
Battery	3.7 V, 300mA

Table 5.3: Power source specifications

5.3.4 | Power Distribution

A spacecraft's power distribution system plays a major role in developing a proper distribution network for power supply. It consists of connections, preventing faults. The load profile plays an important role in the designing a power distribution subsystem. A centralized power distribution system was used for our model. In this approach the entire power is regulate in the main bus. A centralized bus eliminates the need for a separate EPS for all the components. A regulated 3.7 V regulated system bus was used for this purpose. To finalize this electrical Load profile was calculated from Table 1.

Electrical Load Profile

Possibilities

Low voltage DC: 1.4 V

High voltage DC: 3.7 V

Centralized Power Distribution Control from the main Bus is to be used

3.7 V regulated System Bus

5.3.5 | Power Regulation and Control

Peak Power Tracker is used for power control as it extracts the exact power that is required up to the array peak power. A PPT is a dc-dc converter which operates in series with the solar array. It has a lot of advantages:

- It has also been used in the missions like PCBSAT
- It operates in series with the solar array.
- It is good for missions under 5 years and gives more power at BOL

Also a fully regulated electrical bus voltage control is selected as it is a lower power mission.

Also a parallel battery recharge subsystem is used.

5.3.6 | Finalized Components/Design for Power System in Femto Satellite

Based on the power budget calculation, the following components were selected to be used in our mission.

- Lithium-Ion Coin Battery

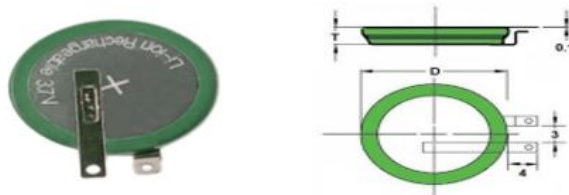


Figure 5.4: Lithium-Ion Coin Battery

Model Number	RJD3048ST1
Dimensions	30mm Diameter
Weight	9.3 gm
Height	4.8 mm
Nominal Voltage	3.7VDC (4.2VDC to 3.0VDC)
Capacity	290 -300 mAh
Operating Temperature Range	-20°C to +60°C
Storage Temperature Range	-20°C to +60°C (one month)
Charging current	0.5CA
Charging Time	< 3.0 hours
Charging method	Constant Current/ Constant Voltage (CCCV)
Certification	UL1642 – MH28281 Markings Standard (bare cells) Non-Standard
Cell Life	500 Cycles

Table 5.4: Specifications: Lithium-Ion Coin Battery

■ Gallium Arsenide Solar Panel

Figure 5.5: Gallium Arsenide Solar Panel

Specifications:

Brand Name	CBE
Work Time	24 hrs
Efficiency	18.5% efficiency
Maximum System Voltage	1000 V DC
Maximum Series Fuse Rating	20 A
Tolerance	0/+3W
Type	Gallium Arsenide
Operating Temperature	-40°C to +80°C

Table 5.5: Specifications: Gallium Arsenide Solar Panel

■ Design Layout

3.7 V Regulated System Bus control

Centralized Power Distribution Control

Peak Power Tracker is used for power control as it extracts the exact power that is required up to the array peak power.

5.4 | Power Budget: HUB

5.4.1 | Power Requirement of all Subsystems

The power required by all the subsystems for the hub design was collected and summarized as follows:

Table 5.6: Power Required by all the subsystems for Hub

Component	No. of Components to be used	Low Voltage V	Average Voltage V	Peak Voltage V	Current mA	Power consumed based on average voltage mW	Power consumed on peak voltage mW
Micro-controller- 512MB flash cp400.85	1	3.1	3.3	5	NA	700	1000
Magnetometer	1	1.95	2.4	3.6	0.9	2.16	3.24
Vector nav iIMU	1	3.3	NA	3.3	45	NA	185
Magnetorquers Satbus MTQ M3x	1	NA	NA	5	NA	800	1000
Reaction wheels RS100	1	NA	NA	5	NA	NA	700
Transceiver with becon UHF	1	5	9.5	14	NA	NA	1000
Transceiver CC2500	1	1.8	2.7	3.6	100	NA	100
Propulsion System PUC-184-SO2	1	NA	NA	12	NA	NA	5300
Position Determination: GPS receiver SGR-05P	1	NA	NA	3.3	NA	NA	1000

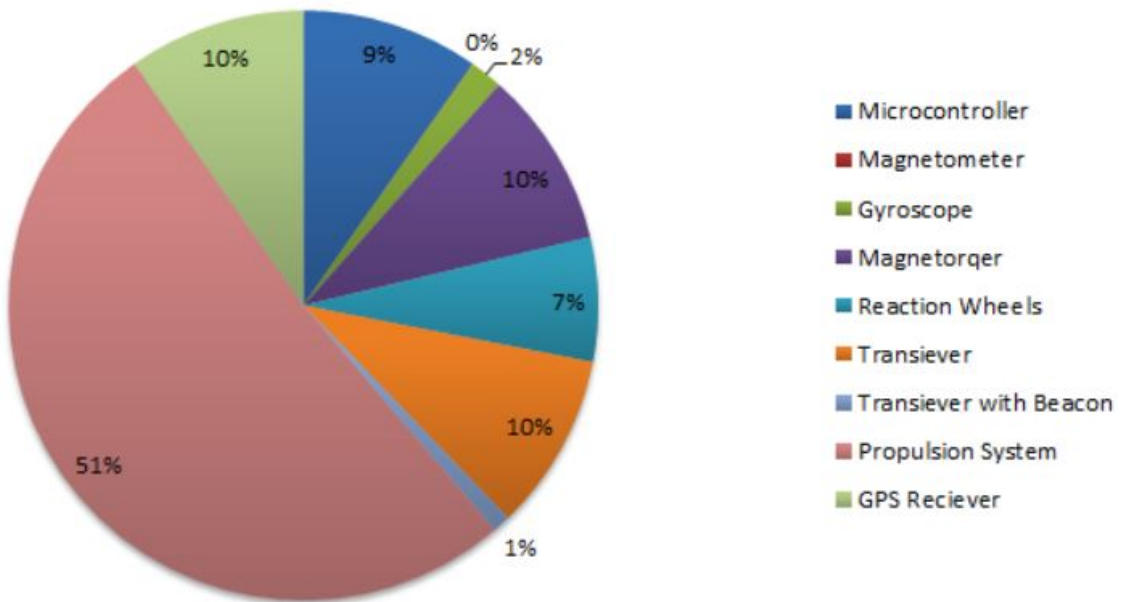


Figure 5.6: Power consumption for HUB

Based on the sum of the power requirement of all the subsystems, a rough power requirement with a buffer of 20% was considered to be 12W based on the peak voltage. In a practical scenario, not all the components will be operating at the same time.

5.4.2 | Power Generation

Generating Power in space environment has always been a complex concept of research. One of the major sources of energy that can be utilized for generating power in space, is the Solar Energy. Based on our mission objectives, the orbit selected was sun synchronous orbit, which eliminated the eclipse occurrence. The major source of power generation was considered to be solar energy. This energy is generated using solar panels mounted on the satellite body. In order to select the solar panels for this mission, the amount of power required to be produced by the solar panel needs to be calculated as a part of the power budget and a panel that satisfies our mission objectives is to be selected (28).

Amount of Power to be produced by the Solar Array P_{sa}

The amount of power needed to be generated by the panels was calculated using the equations below to be 1.5 W.

$$P_e = P_d = 12W \text{ (Based on Peak Voltage from Table 1)}$$

$$T_e = T_d = 100\text{min} \text{ (orbital period)}$$

Assuming Peak Power Tracking Regulation Scheme

$$X_e = X_d = 0.8 \text{ (Efficiencies of the power distribution Path)}$$

$$P_{sa} = \frac{\frac{P_e T_e}{X_e} + \frac{P_d T_d}{X_d}}{T_d} = 35W$$

Where,

P_{sa} = Amount of power to be produced by the Solar Array

P_e & P_d = Spacecraft power requirements (Excluding regulation and battery charging losses)

T_e & T_d = Lengths of the period per orbit

X_e & X_d = Efficiencies of the power distribution paths

Ideal Power Production**Estimating Solar Cells power output P_o , with the sun normal to the surface of the cells**

In order to determine the power output that can be produced by a solar cell, here the gallium arsenide solar panel is selected. This panel was selected due to the various advantages that it offers for our mission. It has a much better efficiency in comparison to silicon solar panel. But it is 3 times much costlier than the traditional silicon solar panel (28). In this step, to identify the correct type of panel to suit our mission the following table was considered as a source of reference.

It was found out that the achieved performance efficiency for gallium arsenide panel was found to be 18.5% (28). Using this information the ideal cell power output per unit area can be calculated as follows. (Efficiency of 18.5%)

$$\text{Solar Constant} = 1,367W/m^2$$

$$P_o = 0.185 * 1,367 = 253W/m^2$$

TABLE 11-35. Performance Comparison for Photovoltaic Solar Cells. Note that the stated efficiencies are for single solar cells, not solar arrays.

Cell Type	Silicon	Thin Sheet Amorphous Si	Gallium Arsenide	Indium Phosphide	Multijunction GaInP/GaAs
Planar cell theoretical efficiency	20.8%	12.0%	23.5%	22.8%	25.8%
Achieved efficiency: Production Best laboratory	14.8% 20.8%	5.0% 10%	18.5% 21.8%	18% 19.9%	22.0% 25.7%
Equivalent time in geosynchronous orbit for 15% degradation – 1 MeV electrons – 10 MeV protons	10 yr 4 yr	10 yr 4 yr	33 yr 6 yr	155 yr 89 yr	33 yr 6 yr

Figure 5.7: Solar Panel Selection (Reference: Space mission Design and Analysis, Wiley J Larson, James R Wertz)

Realistic Power Production

Realistic power production capability of the manufactured solar array is the most important parameter to be calculated. In real-time there are various factors that affect the actual power produced and is far different from the idealistic case. Here comes the concept of inherent degradation, ld. The various factors that account for inherent degradation is due to design and assembly, temperature of array etc (28).

Beginning of Life Power Production Capability P_{bol}

Radiation damage severely reduces a solar array's output voltage and current. Life degradation, LD occurs because of thermal cycling in and out of eclipses, micro-meteoroid strikes, plume impingement from thrusters etc.

$$I_d = 0.77$$

At sun synchronous orbit, $\theta = 0$

$$P_{bol} = I_d \cos \theta$$

$$P_{bol} = 2530.77 \cos 0 = 194.81 W/m^2$$

There is a code mistake in the above two formulae

Where,

θ = Sun Incidence Angle

$\cos \theta$ = Cosine loss

Maximum power will be produced when the Sun's rays are perpendicular to the solar array's surface.

End of Life Power Production Capability P_{eol}

Radiation damage severely reduces a solar array's output voltage and current. Life degradation, L_d occurs because of thermal cycling in and out of eclipses, micrometeoroid strikes, plume impingement from thrusters etc. For gallium-arsenide cells in LEO, the degradation is about 2.75% per year, of which radiation causes 1.5% per year (28).

The actual lifetime degradation can be estimated using

$$L_d = (1\text{-degradation/yr})^{\text{satellitelife}} \quad (\text{ActualLifetimeDegradation})$$

$$L_d = (1-0.0275)^1 = 0.9725$$

The array's performance per unit area

$$P_{eol} = P_{bol} L_d$$

$$P_{eol} = 189.45 \text{ W/m}^2$$

Area of the solar Array required

The area required to support the power requirement of the subsystem is

$$A_{sa} = \frac{P_{sa}}{P_{eol}} = \frac{35}{189.45} = 1847 \text{ cm}^2$$

Mass of the solar Array required

The mass of the required solar panel can be calculated as follows:

$$M_{sa} = 0.04 P_{sa} = 0.04 * 12 = 1.4 \text{ kg}$$

5.4.3 | Power Storage

For our mission we considered a secondary battery that was rechargeable using solar energy for power. Lithium ion battery was selected, because with 65% volume advantage and a 50% mass advantage (28). The Depth of Discharge (DOD) for Lithium-Ion Battery is assumed to be 30%. After developing a general idea, the calculation to select the battery was carried out as follows:

Battery Selected	Lithium Ion Battery
Nominal Voltage	upto 14 V _{dc}
No of Batteries N	
Transmission Efficiency Between the battery and Load	n=0.9
Depth of Discharge(DOD)	0.3
Battery	12 V, 6200 mA

Table 5.7: Types of Power sources used in Previous Missions

5.4.4 | Power Distribution

A spacecraft's power distribution system plays a major role in developing a proper distribution network for power supply. It consists of connections, preventing faults. The load profile plays an important role in the designing a power distribution subsystem. A centralized power distribution system was used for our model. In this approach the entire power is regulated in the main bus. A centralized bus eliminates the need for a separate EPS for all the components. A regulated 3.7 V regulated system bus was used for this purpose. To finalize this electrical Load profile was calculated from Table 3.

Electrical Load Profile

Possibilities

- Voltage dc : 1.7 V
- Voltage dc : 14 V

Centralized Power Distribution Control from the main Bus is to be used

Here a 12 V regulated System Bus is to be used even though the high voltage as step down converter will be used to reduce the power.

5.4.5 | Power Regulation And Control

Peak Power Tracker is used for power control as it extracts the exact power that is required up to the array peak power. A PPT is a dc-dc converter which operates in series with the solar array. It has a lot of advantages:

- It has also been used in the missions like PCBSAT
- It operates in series with the solar array.
- It is good for missions under 5 years and gives more power at BOL

Also a fully regulated electrical bus voltage control is selected as it is a lower power mission.

A parallel battery recharge subsystem is used.

5.4.6 | Finalized Components/Design for Power System in HUB

Based on the power budget calculation, the following components were selected to be used in our mission.

- Lithium-Ion Battery



Figure 5.8: Lithium-Ion Battery

Model Number	1826120030
Dimensions	112.5 x 19.05 x 71 mm
Nominal Voltage	12 VDC (4.2VDC to 3.0VDC)
Capacity	6200 mAh
Cell Life	100 Cycles

Table 5.8: Specifications: Lithium-Ion Battery

■ Gallium Arsenide Solar Panel



Figure 5.9: Gallium Arsenide Solar Panel

Brand Name	CBE
Work Time	24 hrs
Efficiency	18.5% efficiency
Maximum System Voltage	1000 V DC
Maximum Series Fuse Rating	20 A
Tolerance	0/+3W
Type	Gallium Arsenide
Operating Temperature	-40°C to +80°C

Table 5.9: Specifications: Gallium Arsenide Solar Panel

- XL6009 Dc to DC voltage converter adjustable step up boost power converter

XL6009 DC DC Boost Module

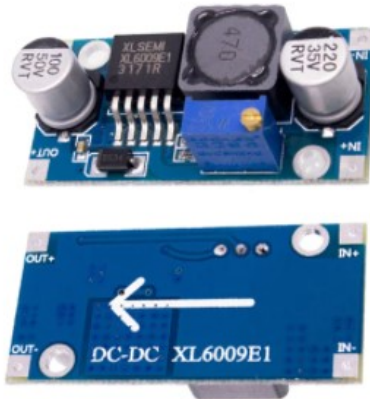


Figure 5.10: XL6009 DC - DC voltage converter

Model Number	DSN6009 boost module
Dimensions	43 x 20 x 12 mm
Weight	3 gm
Module Properties	Non-isolated boost (BOOST)
Rectification	Non-Synchronous Rectification
Input Range	3V 32V
Output Range	5V 35V
Conversion efficiency	<94% (greater the pressure, the lower the efficiency)
Switching frequency	400KHz
Load and Voltage Regulation	+/-0.5%, +/-0.5%
Operating Temperature	-40 degree to +85 degree

Table 5.10: Specifications: XL6009 DC to DC voltage converter

- Adjustable output 1.5-amp sip-mount DC to DC converters

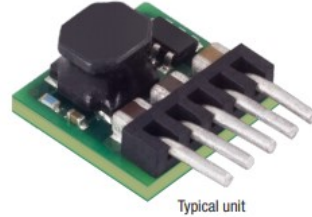


Figure 5.11: OKR-T/3 series DC - DC voltage converter

Specifications:

Model Number	OKR-T/3 series
Dimensions	10.4 x 10.16 x 6.1 mm
Weight	2 gm
Certification	to UL/EN/IEC 60950-1 safety standards, 2nd edition, RoHS-6 hazardous substance compliance
Input Range	4.5-14 VDC
Output Range	0.591-6.0 VDC
Conversion efficiency	93%
Operation	600 KHz

Table 5.11: Specifications: Xl6009 DC to DC voltage converter

- Design Layout

12 V Regulated System Bus control

Centralized Power Distribution Control

Peak Power Tracker is used for power control as it extracts the exact power that is required up to the array peak power.

5.5 | Attitude Determination and Control System For Femto satellite

For a remote sensing mission, it's requisite that the payload (camera) points to the region of interest and the tumbling of the satellite be reduced right after deployment. Attitude determination and control is the system responsible for the stabilisation of satellite and to maintain the desired orientation. Space environment being unpredictable and harsh, it is quite challenging to ensure proper functionality of the femto satellite. High accuracy should be achieved at the same time satisfy the mass and power restraints. The advent of MEMS sensors is a major catalyst for incorporating sophisticated designs in a femto satellite.

PCBsat – Sun sensors for Attitude determination, Passive aerodynamics for attitude control

Wikisat – Photodiode sun sensors for Attitude determination, Magnetorquer (active) and four magnets (passive) for attitude control

Sprite chipsat – Magnetometer, gyroscope for attitude determination

5.5.1 | Altitude Determination System: ADS

Miniaturised sensors and Commercial-off-the-shelf components (COTS) are exploited for determining the attitude. The attitude of a satellite is defined by three axes: yaw, pitch and roll. Sensors measure a physical quantity based on which the orientation of the satellite with respect to a celestial body is found. There is a profusion of sensors available for e.g., sun sensors, earth sensor, geo-magnetic sensor. The attitude of the satellite cannot be estimated by using a single sensor and thus, more than two sensors are required.

Sun sensors, magnetometer and gyroscope were chosen for 3-axis attitude determination taking into consideration the constraints of a femto satellite. Earth sensors, though having a better accuracy than the other sensors, are bulky and hence cannot be included into a femto satellite. The components were selected based on the criteria of minimum power/mass with maximum efficiency. The sensors must be calibrated well in advance to remove bias, body frame deflections and interference from various sources for efficient performance (46).

5.5.1.1 | Sun sensor

Sun sensor is commonly used in attitude determination to compute the orientation of satellite based on the position of the sun. Since a typical sun sensor from the market isn't suitable in terms of volume, two photodiodes are chosen to perform the function of a sun sensor at a much lower cost than the available sun sensors. The basic principle is that the angle of the incident sunlight can be calculated from the current produced by the diode. By having two diodes, orientation w.r.t. sun is determined. Being a sun synchronous orbit, eclipse period doesn't occur, i.e., illumination from the sun is available all throughout the orbital period. As an extension, the current from the solar panels can be evaluated to provide redundancy in estimating the sun vector and have a better accuracy(50). The obtained angle is compared with the sun position data to estimate the sun vector, which can be computed based on the orbital time and position of sun with respect to earth or retrieve the data stored in the on-board memory.

OPR5910 photodiodes

- Dimensions: 3 x 3 x 1.47mm
- Temperature: -50 to 125 C
- Mass: 1.46g

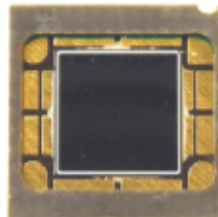


Figure 5.12: OPR5910 photodiode based sun sensor

5.5.1.2 | Magnetometer

As we have chosen LEO, the magnetic field strength of earth at 790km is quite significant and hence we can measure the magnetic field to find out the attitude. Magnetometer measures the local magnetic field strength in all the three axes. Magneto resistive materials are present within the sensor wherein the resistance of the material changes proportional to the strength of the ambient magnetic field. The obtained values are then compared with the IGRF data (Earth's magnetic field model) present in the on-board

memory. The IGRF-2015 data has the coefficients and the earth vector is calculated using the values measured by the magnetometer and the coefficients.

Xtrinsic MAG3110 3-axis digital magnetometer

- Specs: 2.4V, 8. 6A @ 1Hz
- Dimensions: 2 x 2 x 0.85mm
- Temperature: -40 to 85 C
- Mass: <1g

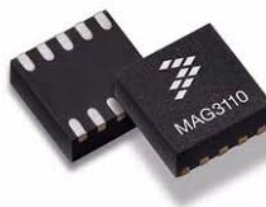


Figure 5.13: Xtrinsic MAG3110 3-axis digital magnetometer

5.5.1.3 | Gyroscope

The gyroscope is used to measure the spin rate of the satellite. The spin must be brought down to 0 as the camera should always point the earth. Gyroscopes have the satellite body as the reference frame. However, these sensors are the major point source of noise in attitude estimation. Thus, a complex and efficient algorithm is required to calibrate and compute the output values from the gyro. The vibrating material inside the gyroscope generates a proportionate change in electrical signal whenever a motion occurs and the angular velocity is determined.

ITG 3701 3-axis gyroscope

- Specs: 2.4V, 8. 6A @ 1Hz
- Dimensions: 2 x 2 x 0.85mm
- Temperature: -40 to 85 C
- Mass: <1g



Figure 5.14: ITG 3701 3-axis gyroscope

5.5.2 | Altitude Control System: ACS

Once the attitude is estimated, the controller computes the deflections from the desired values and are given to the actuators which controls the orientation of satellite by performing the required manoeuvres. There are two types of control: Passive and active control system.

Passive: Doesn't consume any power but the accuracy and control over the attitude is very low and thus cannot suit our application.

Active: Magnetorquers, reaction wheels, thrusters are generally used in this case. The latter two are heavy and requires more power, hence not considered. Magnetorquers seemed to be more promising and compact for a femto satellite demanding significant accuracy.

5.5.2.1 | Magnetorquers

Magnetorquers uses the magnetic field of earth and the dipole moment from the coil to generate the torque. The drivers use PWM to vary the current given to the torquers thus providing the required torque.

$$\text{Torque} = \text{Dipole moment} \times \text{Earth's magnetic field}$$

The torque produced is perpendicular to the earth's magnetic field. Three axis control is achieved here by using two-ferrite core rods and one air core coil. As the torquers available in the market didn't meet our requirements in terms of mass and volume, we designed our own torquer by approximating the external torques that might disturb the femto satellite's attitude. It is known that the atmospheric drag is less as the orbit is 790km from the surface of the earth. The required dipole was estimated to be 0.01Am^2 . Once the required dipole is estimated, the number of turns and the mass required for the torquers are computed. Based on the dimensions of the femto satellite, the rod length of 35mm was chosen. 30mA was allocated for each torquer.

Ferrite rod design(40):

I = current

L = Length of the torquer

r = Radius of the torquer rod

N_d = demagnetisation factor

M = magnetic dipole moment

$$N_d = \frac{4[\ln \frac{L}{r} - 1]}{\left(\frac{L}{r}\right)^2 - 4 \ln \frac{L}{r}}$$

$$M = \pi r^2 NI \left(1 + \frac{v_r - 1}{1 + (M_r - 1)N_d} \right)$$

The above formula is used to calculate the number of turns (N) required.

Current (mA)	30
Dipole(Am²)	0.01
Length(mm)	35
Diameter(mm)	3
Number of turns	770
Mass of the magnetorquer(g)	1.9

Table 5.12: Magnetorquer parameters - Ferrite core

Air-core design(39):

A, Area of the air-core = 35mm x 35mm

$$M = NIA$$

Similarly, the number of turns for the air core is calculated by plugging in all the known values in the above equation.

Current (mA)	30
Dipole(Am²)	0.01
Dimensions(mm)	35 x 35
Number of turns	273
Mass of the magnetorquer(g)	2

Table 5.13: Magnetorquer parameters - Air-core

Once the number of turns is computed, the resistance of the wire and the total power is evaluated using the formula:

$$\text{Resistance}(R) = \text{Resistivity}_{\text{wire}} * \text{Length}_{\text{wire}} / \text{Area}_{\text{wire}}$$

$$P = I^2 x R$$

TOTAL PEAK POWER CONSUMPTION: 180mW

Aluminium wire is used as it has less mass density when compared to copper (8000kg/m³). PC-47 is used as the ferrite core as it has very low power loss. The rods are placed on adjacent sides of the femto satellite and the coil is placed between the PCB and solar panel side(36)(38).

Density(kg/m³)	2700
Resistivity(Ω m)	2.8x10 ⁻⁸
Wire diameter(mm)	0.13

Table 5.14: Aluminium

Density(kg/m³)	4900
Relative permeability	2500

Table 5.15: PC-47



Figure 5.15: Ferrite core and air core magnetorquers

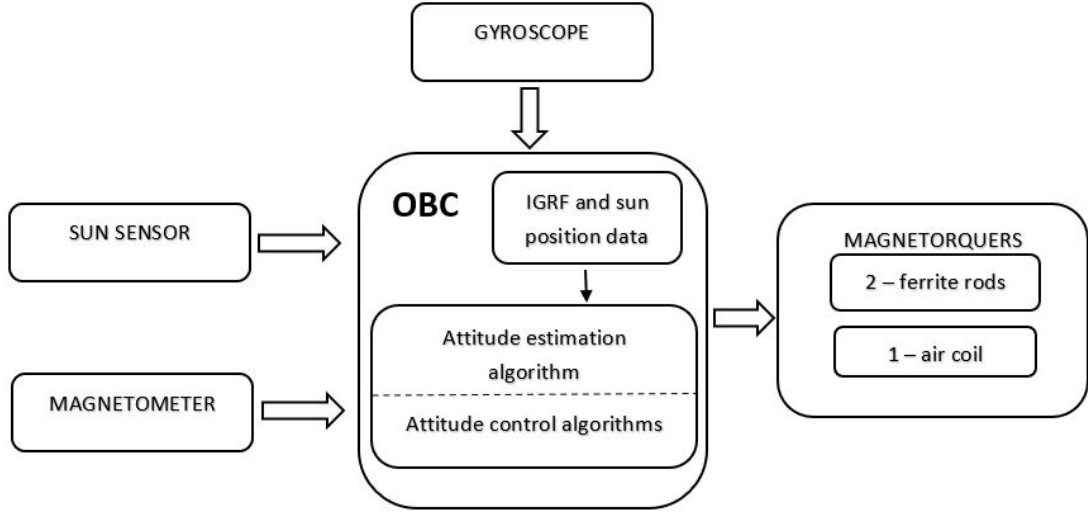


Figure 5.16: Basic flow diagram of ADCS

5.5.3 | Algorithm

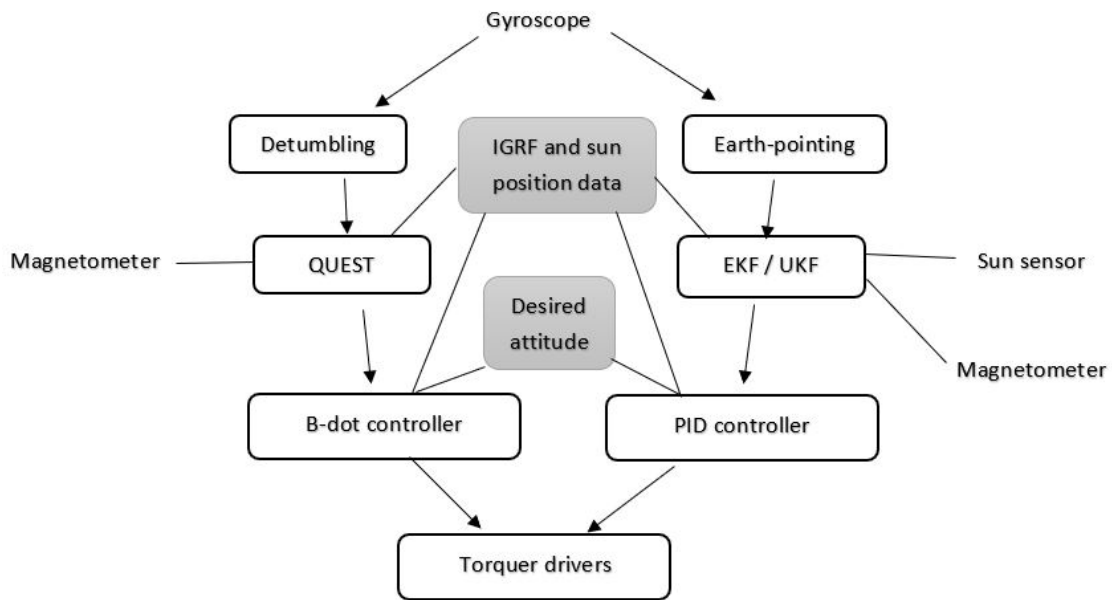
The earth and satellite body reference frames are considered to proceed with the estimation and control. To estimate the attitude, quaternion representation is used as it is found to be more accurate. Kalman filter takes a predictive approach to estimate the attitude and then compares it with the measured data to decrease the error. The effect of noise is minimized by implementing extended Kalman filters. UKF (Unscented Kalman filter) can be used instead of EKF for better results(51).

ADCS has two major modes: Detumbling and the earth pointing mode[10].

Detumbling: During deployment satellite encounters tumbling effect which must be lowered. Gyroscope and magnetometer are used here. QUEST (quaternion estimation) provides higher accuracy for computing the attitude. As the computational cost is quite high, this cannot be utilized throughout the orbital lifetime. B-dot control algorithm which tries to bring down the angular velocity of the satellite is employed as soon as the femto satellites are deployed. The derivative of earth's magnetic field is calculated and based on the value, a dipole is applied in the opposite direction to counter the effect(45).

Earth pointing: In this mode, the system ensures that the camera points to earth. The attitude is estimated using the quaternions and the Kalman filter by combining all the values measured by multiple sensors. The error between desired and estimated attitude is given to the controller. Proportional Integral Derivative, PID controller is implemented

for attitude control, being the most common controller used for space applications. The main objective of this controller is to limit the pointing error(46).



5.6 | Attitude Determination and Control System For Hub

The 6U deployer has two main function: release the femto satellites and act as the mother hub. Thus, it is inevitable that the orientation of the satellite should be maintained all the time. As a hub, it is required that the antenna points to the antenna of the femto satellite during communication and points to the earth (ground station antenna) to achieve maximum information transfer with lesser loss. ADCS ensures the above activities by employing a variety of sensors and actuators for quality estimation and control. The components available in the market are considered as the restraints weren't much compared to a femto satellite.

Sun sensors, magnetometers, gyroscopes were decided to be the sensors for the attitude determination.

5.6.0.1 | Sun sensors

One quadrant photodiode and four photodiodes(46) are placed on each face of the CubeSat except on the side pointing the earth. Quadrant photo-diode(48) acts as a position-sensing device wherein the intensity of sunlight in the four slots are computed. The values from all the sun sensors are collected and compared with the sun position data computed by the OBC to determine the sun vector.



Figure 5.17: OPR5925 quadrature photodiode and SLCD-61N8 photodiode

5.6.0.2 | Integrated Inertial Measurement Unit (IMU)

3-axis magnetometer measures the local magnetic field in three axes and along with the Earth's field model the orientation with respect to earth can be found. Accelerometers are used to measure the linear velocity whereas 3-axis gyroscope computes the angular

velocity in all the three axes (roll, pitch and yaw). The **Vector Nav VN-100** contains 3-axis magnetometer, 3-axis gyroscope and 3-axis accelerometer. This product also has an inbuilt 32-bit processor for attitude estimation (with Extended Kalman filter) and on-board geo-magnetic model of earth. Xtrinsic MAG 3110 Magnetometer is also used a redundant sensor to achieve a higher accuracy.

- Specs: 5V, 45mA
- Dimensions: 24 x 22 x 3mm
- Mass: 3.5g



Figure 5.18: Vector Nav VN-100 iIMU

The correction measures for torques and tumbling due to the external disturbances are done by the actuators.

5.6.0.3 | Magnetorquer

Once the change in the orientation from the desired value is computed, the drivers provide the current to generate the required dipole. The torque is created when the dipole moment interacts with the local earth's magnetic field. Integrated PCB based **Satbus MTQ M3x magnetorquer** is chosen as it is compact and provides 3-axis control.

- Specs: 0.86W peak
- Dimensions: 96 x 94 x 17 mm
- Mass: 200g

5.6.0.4 | Reaction wheels

Reaction wheels are generally used to store the angular momentum and have very high accuracy when compared to torquers. **RS-100** is an integrated reaction wheel motor; a single spherical motor that works similar to 3 magnetorquers.

- Power: <1W
- Mass: 400g



Figure 5.19: Satbus MTQ M3x magnetorquer and RS-100 reaction wheel

5.6.0.5 | Algorithm

The sensors must be calibrated to remove the bias errors. For attitude estimation, quaternion representation and extended Kalman filter is used (implemented in the Vector Nav VN-100 IC). Apart from EKF, QUEST (Quaternion estimation) algorithm is applied for higher performance, especially during the detumbling mode.

Detumbling mode: To mitigate the tumbling effect, B-dot algorithm is utilized where the derivative of magnetic field (along with gyroscope) is obtained to bring down the angular velocity to 0.

Earth-pointing mode: Once the attitude is estimated, the deviation from the desired attitude is given to the PID controller which sends the values to the torquers and reaction wheels making the satellite point towards the earth. (46)(51)

5.7 | Position Determination System For Femto satellite

The locations of the satellites are determined using tracking from ground stations. The ground stations use mechanisms such as radar, signal Doppler, and laser reflectors to pinpoint the position of a satellite and to maintain an understanding of its orbital elements.

COMPONENT USED FOR POSITION DETERMINATION IN SMALL SATELLITES

- PCB SAT - Position tracking is done by GPS receiver.
- RYE FEM SAT - Position was determined by GPS receiver.
- WIKI SAT - Positioning determination is done by IMU.
- POCKET-PUCP - The position of this satellite is not known and no component is used.
- KICK SAT - Position determination was done by GPS receiver.
- SWIFT - Position determination was done by GPS receiver.
- LEO SPACECRAFT - GPS receivers [5] are now the primary method for performing orbit determination, replacing ground-based tracking methods.

In Earth orbit, on-board position determination can be provided by a GPS receiver with 1.5 m position accuracy. For position sensing, COTS Global Positioning System (GPS) sensors are the best option. Since space-qualified GPS modules are too heavy (30% of the femtosats mass), other civilian versions are suitable from the accuracy point of view, but require radiation hardening and space-suitable software upgrade. Hence, a reliable lightweight GPS sensor is a technology development area [6, 11]. We decided to go for GPS receiver for the position determination of our Femto satellite as well as deployer which is a 6U cube sat.

What is the need of GPS?

1. Doppler shift handling
2. Precise orbit determination
3. Time travelling of satellite
4. Corrects antenna performance

5. On-board interference handling
6. Autonomous orbit control and maneuver planning

How GPS works?

The GPS receiver gets a signal from each GPS satellite. The satellites transmit the exact time the signals are sent. By subtracting the time the signal was transmitted from the time it was received, the GPS can tell how far it is from each satellite [14]. The GPS receiver also knows the exact position of the satellites in the sky, at the moment they sent their signals. So given the travel time of the GPS signals from three satellites and their exact position in the sky, the GPS receiver can determine the position in three dimensions - east, north and altitude.

GPS RECEIVER FOR FEMTO SAT

Model: GNSS200 Series Global Navigation Receiver

The GNSS200 Global Navigation Satellite System (GNSS) receiver is a low mass, low power GNSS receiver for use in (small) satellites. It is designed specifically for use in CubeSat platforms, and it can also be used in conjunction with the iADCS-series of attitude determination and control systems as well as the iACS series of attitude control systems. It offers a multi-constellation output, and the standard version is delivered with a TTL UART output. It is designed to work either with active or passive antennae (to be defined at the time of ordering) and outputs NMEA-compatible data as standard. It is possible to qualify the units for use in larger satellites as well.

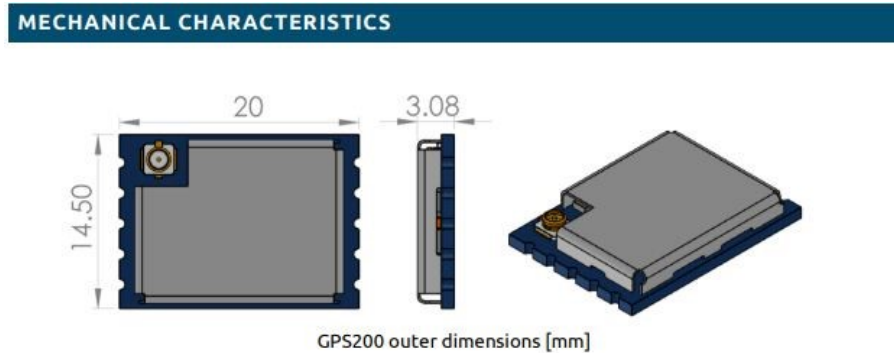


Figure 5.20: GPS200 outer dimensions (mm)

SPECIFICATIONS			
Performance			
Update Rate	> 10	Hz	
Time-to-first-fix (TTFF)	<90 ¹ , <120 ²	s	
Position Accuracy	< 8 ³	m	
Velocity Accuracy	< TBD>	m/s	
Dimensions			
Outer dimensions	20 x 14.5 x 3.1	mm	
Mass	3	g	
Environmental			
Operating temperature	- 40 to + 85	°C	
Radiation tolerance	> 36	krad (Si)	
Communication interface			
TTL UART Baud Rate	9600	bps	
Electrical specifications			
	Min.	Typ.	Max.
Supply voltage	3.25	3.3	3.5
	V		
Power consumption			
	Min.	Typ.	Max.
Acquisition / Tracking	148	157	165
	mW		

Figure 5.21: GPS200 specifications

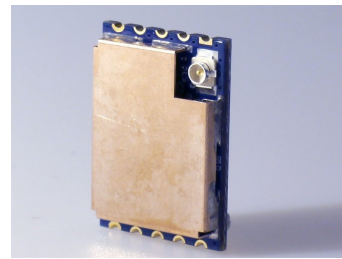


Figure 5.22: GPS200

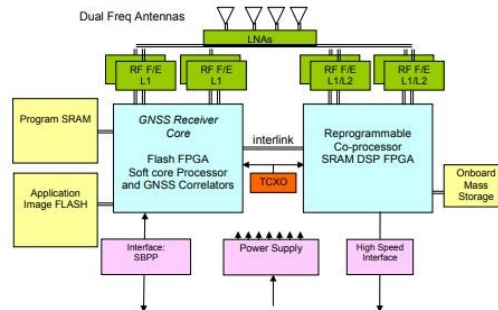


Figure 5.23: GPS data flow diagram

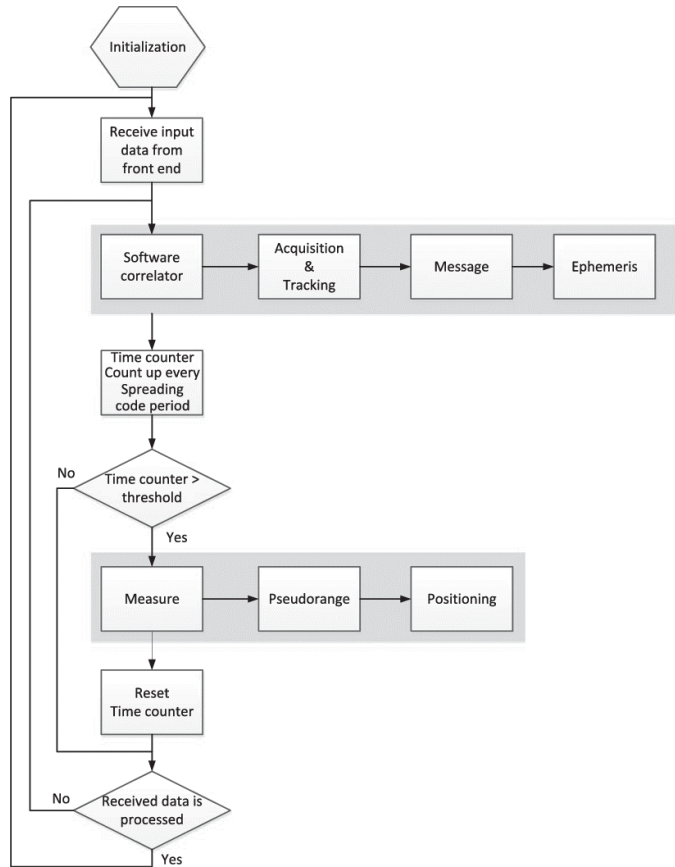


Figure 5.24: GPS flow chart

5.8 | Position Determination System For Hub

MODEL: SPACE GPS RECEIVER SGR-05P

The SGR-05P is a miniaturized single antenna space GPS receiver for providing position, velocity and time in an OEM configuration for the tightest integration requirements on professional small satellites. The SGR-05P comprises of the GPS receiver “engine” from within the SGR-07, and makes use of the host’s regulated power supply and TTL interfaces. The integrator must account for power, EMC, latch-up protection and shielding against radiation, but with the result of a highly compact solution [2, 4, 6].

APPLICATIONS

- Navigation for LEO Missions
- Position, Velocity, Time Determination
- Post-Maneuver Orbit Determination
- Accurate Timing and Synchronization
- Payload Data Time Stamping
- OEM Suitable for Tight Integration on Professional Platforms

Performance Properties	
Number of channels	12
Number of antennas	1
Frequencies & signals	GPS L1 C/A Code
PPS outputs	TTL
SEE mitigation	Yes (SEE & SEL) EDAC protected memories
Typical position*	10 m
Typical velocity *	15 cm/s
TTFF (NVRAM)*	90 s
Time (UTC)*	200 ns
TM/TC interface(s)	TTL UART, TTL CAN

Figure 5.25: SGR-05P Performance properties

Physical Characteristics	
Dimensions (mm)	105 x 65 x 12 mm
Power	1 W (Regulated 3.3V)
Mass	55 g
Temperature	-20° C to +50° C operating -30° C to +85° C non-operating
Random vibration	Tested to 15 Grms in all axes (within SGR-07)
Radiation	Near identical SGR-GEO unit tested to > 11 kRad (Si)

Figure 5.26: SGR-05P Physical characteristics



Figure 5.27: SGR-05P

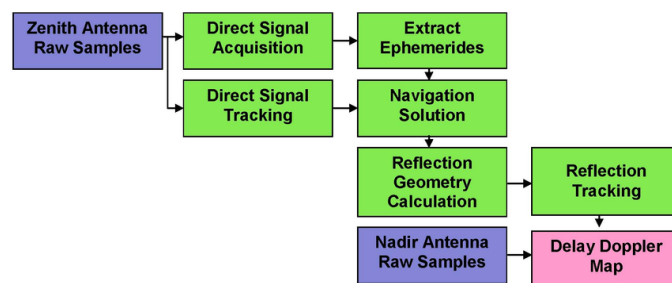


Figure 5.28: Flow diagram

Communication Subsystem

6.1 | Communication systems

The communication system is the most important part of the satellite. It establishes a way of receiving and transmitting data from the ground to the satellites and vice-versa. The signal received by the satellites from the ground stations is known as the **uplink** and the signal transmitted by the satellites to the ground station is known as the **downlink**. This communication is a two-way process. The signal is transmitted as radio waves. When it comes to a communication relay model, timing and attitude play a major role. The femto satellite sends housekeeping and payload data to the Hub, which the Hub then sends to the ground during the visibility window, which in our mission on an average is 11.6 minutes. Lossless transmission of data is key for the success of the mission. Hence a smart choice of components is required.

6.2 | Objectives

The main objective of the communication system is to establish a way to exchange information between the ground station and the satellites. This was planned to be done in two steps considering that the free space loss would be minimised.

- 1.Femto satellite to Hub
- 2.Hub to ground Stations

6.3 | Communication Flow

- Once the femtosats are deployed, imaging operations begin. When the ADS sensors on each femtosatellite indicate that the cameras are facing towards the Earth, a picture will be taken which is compressed to a nominal size and is fed to CC1101 transceiver (UHF band), and is stored in RAM until the femtosat receives the transmission command from the Hub.
- The Hub initiates information transfer by transmitting a TDM-type beacon (TDM-It is a communication process that transmit 2 or more digital signals or analog signals over a common channel) with a synchronization bit and subsequent status bytes that provide instructions to all femtosats.
- When femtosats receive instruction to prompt the exchange information, the Femtosat communication system makes use of two techniques.
 - (i) Matched filtering
 - (ii) Forward error correction (FEC).
- Matched filtering: We use matched filter to overcome low signal to noise ratio (SNR). Aside from improving SNR, matched filtering also makes possible code division multiple access (CDMA), by assigning each femtosat a different pseudo random number (PRN), so that the receiver can “tune” to a particular femto satellite by correlating against its unique code.

6.3.1 | Matched filtering:

The advantages of matched filtering are:

1. This allows all the Femtosatellites on a particular mission to share the same allocated frequency.
2. Eliminates the need for clock synchronization.
3. If the PRN is present, the correlation will be high, even in the presence of substantial noise.

6.3.2 | Aspects

Aspects to be taken care of:

1. Cross-correlations should be close to zero. Unfortunately, it is mathematically impossible to generate code families with perfect zero cross-correlations for all time offsets, so we should check with low and bounded cross-correlations.

2. We should implement CDMA in such a way that, there are minimum PRN interferences.

- Forward error correction (FEC): FEC is widely used in modern digital communication because it allows a receiver to correct errors in a message without having to request a re-transmission. Example: Hamming code.
- In this way the information is transmitted from femtosat to hub through a dipole antenna.
- In order to communicate with the femto satellite we used a UHF transceiver on hub.
- To establish a communication between ground and hub we are going with CC2500 (S band) because of higher downlink frequency.
- Communication protocol used:AX.25
- This data is downlinked through a dipole antenna. In the ground station the data is decoded.
- In order to ensure maximum information transfer, Freespace path loss and link budget calculations are performed.

6.4 | Components

6.4.1 | Criteria for the selection of the components

- Frequency
- Data rate
- Sensitivity
- Free space path loss

The following components were chosen based on the criteria mentioned above.

6.4.2 | Femto-Satellite



Figure 6.1: CC1101 transceiver

CC1101:

- UHF Band.
- High sensitivity.
- half duplex.
- IO pass through modes.
- Long range on open environment , transmission distance can reach 200m straight line.
- Small size (13.5 × 28.2mm).
- Frequency and address can be set.

6.4.3 | Hub



Figure 6.2: CC2500 transceiver

CC2500 2.4GHz Transceiver Features:

- Low power consumption.
- Integrated bit synchronizer.
- Integrated IF and data filters.
- High sensitivity (type -104dBm)
- Programmable output power -20dBm 1dBm
- Operation temperature range : -40 +85 deg C
- Operation voltage: 1.8 3.6 Volts.
- Available frequency at : 2.4 2.483 GHz
- Digital RSSI

UHF transceiver Features:

- Half-duplex communication via single antenna
- Single board radio for telemetry, telecommand and beacon
- In-flight re-configurable beacon period, data rate, frequency, call sign etc.
- In-flight firmware update via RF with backup
- Hardware and software watchdogs

- Customizable beacon message
- Ground to board bridge mode
- RTC with backup power
- Rich telemetry

6.5 | Link Budget

To establish a communication link between a transmitter and a receiver, it is important to carefully adjust the transmit power and the received power required at the receiver for maintaining the desired data rate for a given channel, given a certain thermal noise level at the receiver. This power analysis is required for establishing a link which relies on the link budget. The link budget of a communication system depends mainly on the base station's and the mobile station's specifications, such as the transmit power, antenna gain, signal-to-noise ratio (SNR) and the required throughput of the link.(35) Free space path loss is the loss of signal that occurs during the transmission of the data during uplink and the downlink.

picture :

General formula:

1.Free space path loss:

2.Link budget:

6.5.1 | Link budget calculations

FREE SPACE PATH LOSS:

1.Femto-Hub:

$$= 20(d) + 20(f) + 20 \log\left(\frac{4\pi}{c}\right) = 20(0.5) + 20(437) - 147.55 = -100.79dB$$

2.Hub Ground:

$$\begin{aligned} &= 20(d) + 20(f) + 20 \log\left(\frac{4\pi}{c}\right) - G_{TX} - G_{RX} = 20(567) + 20(2.4) + 20 - 147.55 - 2.1 - 14 \\ &= -100.97dB \end{aligned}$$

LINK BUDGET:

1.Femto-Hub:

$$P_r = P_{TX} + G_{TX} + G_{RX} + 20\left(\frac{\lambda}{4\pi r}\right) = 14 + 2.1 + 2.1 + 20\left(\frac{0.759}{4\pi \times 500000}\right) = -120dB$$

R_x sensitivity= upto-121 dB

Link Margin=1 dB

2.Hub-femto:

$$P_r = P_{TX} + G_{TX} + G_{RX} + 20\left(\frac{\lambda}{4\pi r}\right) = 30 + 2.1 + 2.1 + 20\left(\frac{0.759}{4\pi \times 500000}\right) = -104dB$$

R_x sensitivity=-112 dB

Link Margin=8 dB

3.Hub-Ground:

$$P_r = P_t + 20\left(\frac{\lambda}{4\pi r}\right) = 20 + 20\left(\frac{0.129}{4\pi \times 567000}\right) = -134dB$$

Structural Design

7.1 | Component design

The design considered for the femto satellite are based on dimensions of the components chosen to be mounted on the PCB. Each component is separately designed and assembled in order to bring a visual aspect to the femto satellite. Since the circuits and peripheral components were not considered, approximate dimensions are taken in order to place the components on the PCB. The final design of the femto satellite is dependent only the mass and the volume budget. The electrical design and schematics are not included in the CAD model of the femto satellite. The components of the femto satellite are provided below.

1. Toshiba TCM8230 Imaging Sensor

Mass: 0.18g

Dimensions: 6 x 6 x 4.5mm

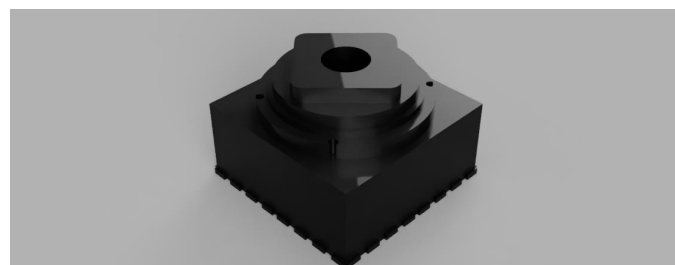


Figure 7.1: Toshiba TCM8230 CMOS imaging sensor

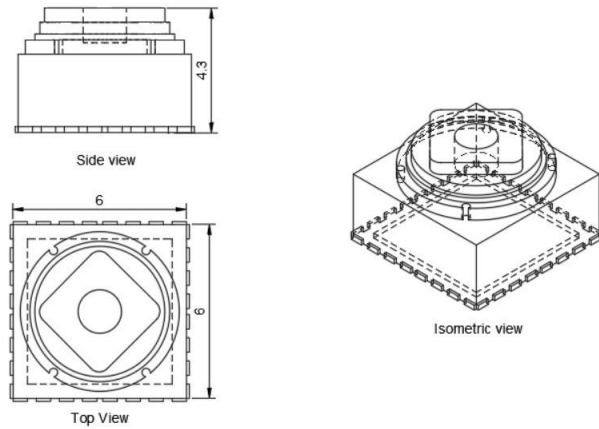


Figure 7.2: Toshiba TCM8230 CMOS imaging sensor

2. Gyro- ITG-3701

Mass: 0.14g

Dimensions: 3 x 3 x 0.9mm

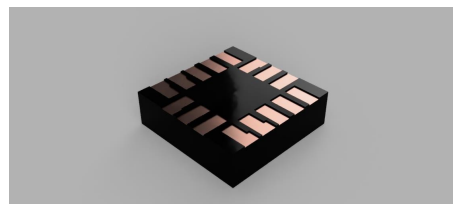


Figure 7.3: ITG-3701 Gyro

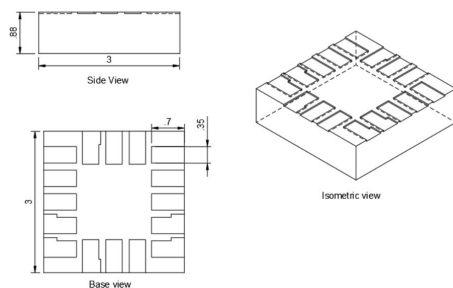


Figure 7.4: Dimensions of ITG-3701 Gyro

3. MSP432 microcontroller with Arm Cortex core

Mass: 1g

Dimensions: 11 x 11 x 3mm

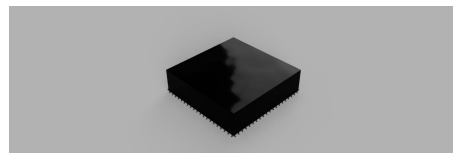


Figure 7.5: MSP432 microcontroller

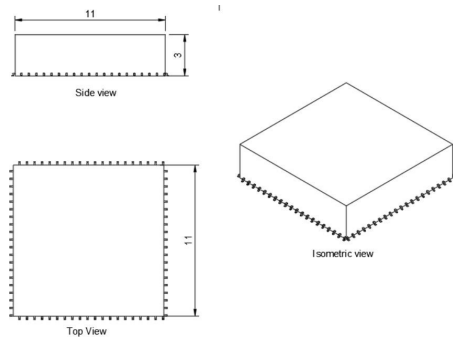


Figure 7.6: Dimensions of MSP432 microcontroller

4. Position Determination sensor- GNS200

Mass: 3g

Dimensions: 20 x 15 x 3.08mm

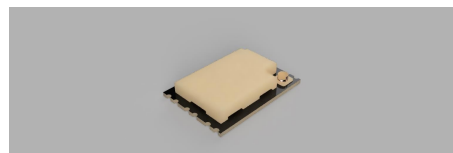


Figure 7.7: GNSS-200 SERIES NAVIGATION RECEIVER

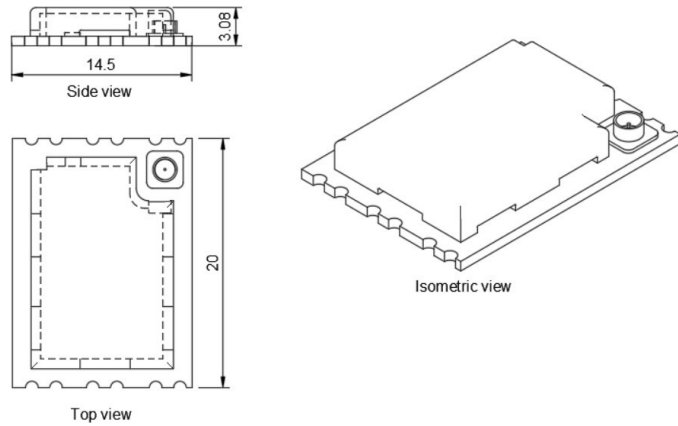


Figure 7.8: Dimensions of GNSS-200 SERIES NAVIGATION RECEIVER

5. Magnetometer- Xtrinsic MAG3110

Mass: 1g

Dimensions: 2 x 2 x 0.85mm

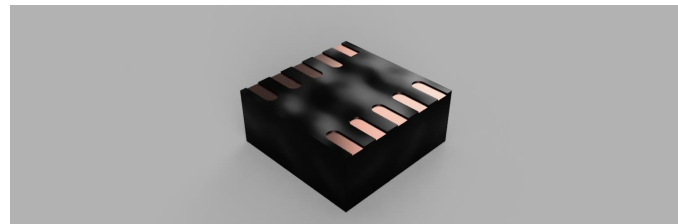


Figure 7.9: Magnetometer- Xtrinsic MAG3110

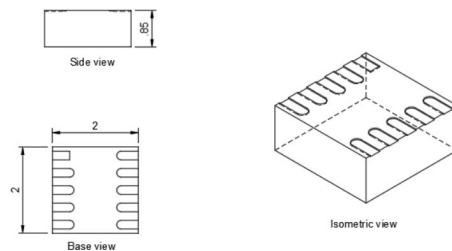


Figure 7.10: Dimensions of Magnetometer- Xtrinsic MAG3110

6. Magnetorquer- rods

Mass: 2.98g

Dimensions: Length - 35mm , Diameter - 3mm



Figure 7.11: Magnetorquer-Rods

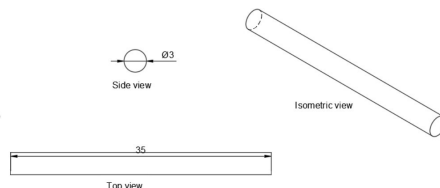


Figure 7.12: Dimensions of Magnetorquer-Rods

7. Sun sensor- OPR5910

Mass: 3g

Dimensions: 3 x 3 x 1.47mm



Figure 7.13: Sun senor- OPR5910

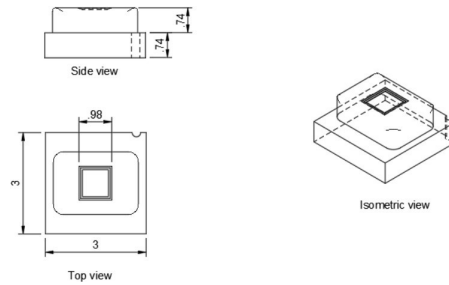


Figure 7.14: Dimensions of Sun senor- OP5910

8. C1101 transceiver

Mass: 3g

Dimensions: 4 x 4 x 0.93mm

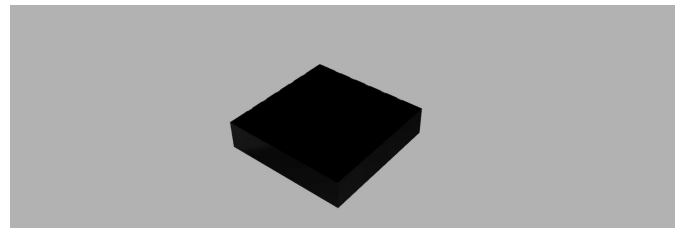


Figure 7.15: C1101 transceiver

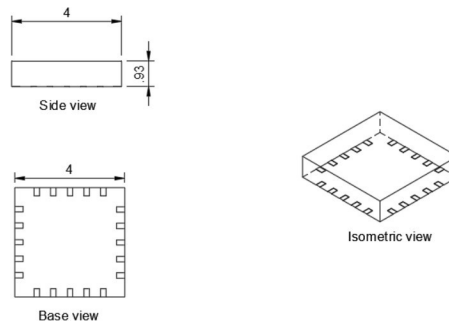


Figure 7.16: Dimensions of C1101 transceiver

9. Air core coil

Mass: 5g

Dimensions: 35 x 35 x 2mm



Figure 7.17: Air core coil

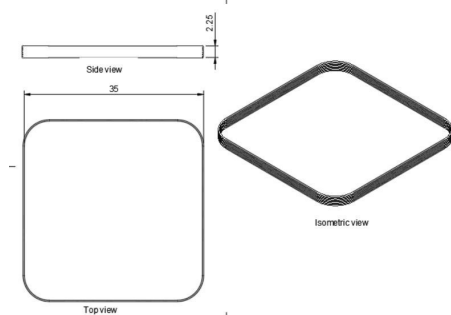


Figure 7.18: Dimensions of Air core coil

10. Driver circuits

Mass: 1g

Dimensions: 2 x 2 x 0.5mm

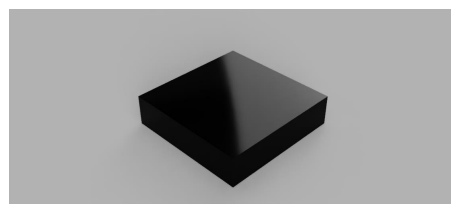


Figure 7.19: Driver circuit

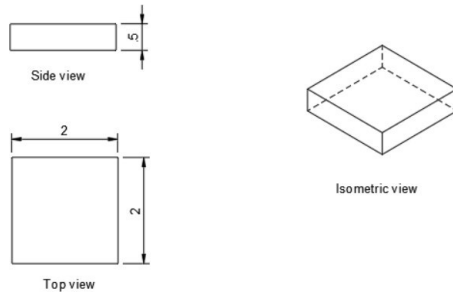


Figure 7.20: Dimensions of Driver circuit

11. Li-ion coin battery- RJD3048ST1

Mass: 9.3g

Dimensions: Height - 4.8mm , Diameter - 30mm



Figure 7.21: Li-ion battery-RJD3048ST1

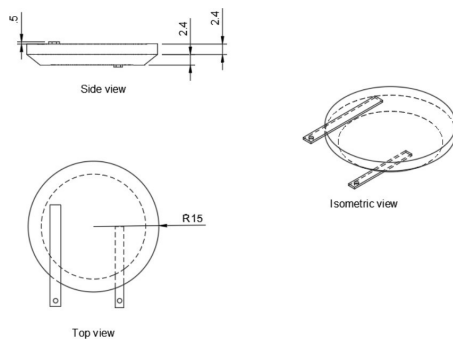


Figure 7.22: Dimensions of Li-ion battery-RJD3048ST1

12. Gallium Arsenide Solar panel

Mass: 60g

Dimensions: 133 x 60mm



Figure 7.23: Gallium Arsenide Solar Panel

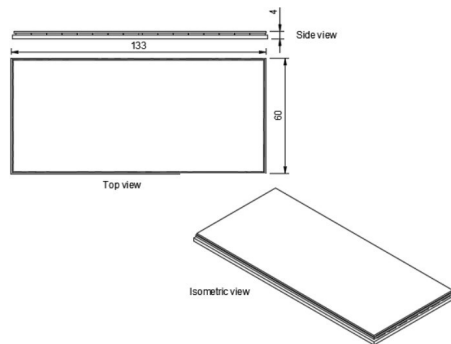


Figure 7.24: Dimensions of Gallium Arsenide Solar Panel

13. PCB (Surface mount)

Mass: 0.14g

Dimensions: 3 x 3 x 0.9mm

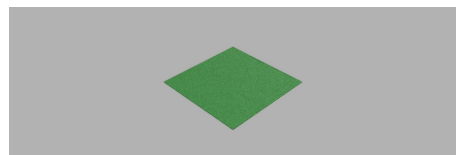


Figure 7.25: PCB

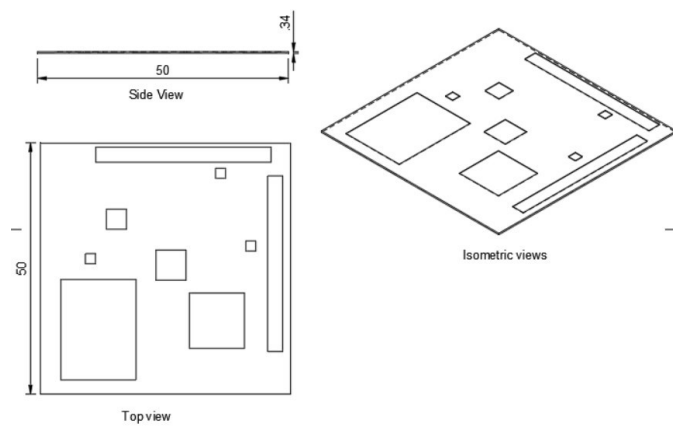


Figure 7.26: Dimensions of PCB

7.1.1 | Final design

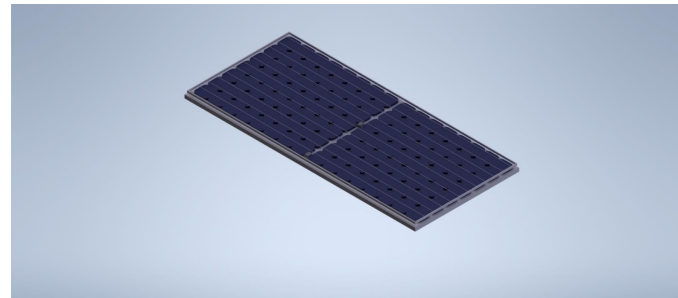


Figure 7.27: Final design 1



Figure 7.28: Final design 2

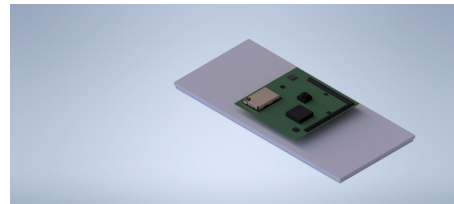


Figure 7.29: Final design 3

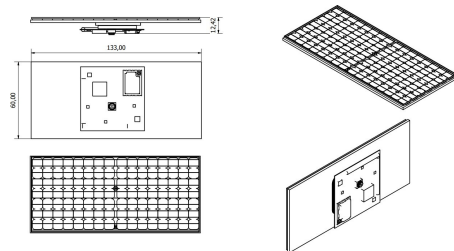


Figure 7.30: Dimensions of Final design

7.2 | Mass and Volume budget

Femto-satellite		Mass and Volume Budget	
Sub-System	Component Name	Specified Mass (g)	Dimensions (mm)
Power	RJD3048ST1 Lion coin Battery/250mAh Li-ion Battery at 3.7V	9.3	Diameter :30 mm/Height 4.3 mm
	Galium Arsenide Solar Panel	60	79cm^2
Image sensor	Toshiba TCM8230	0.18	6 X 6 X 4.5
Antennae	C1101 + dipole	5	4 x 4 x 0.93
GPS sensor	GNSS-200 SERIES NAVIGATION RECEIVER	3	20 x 15 x 3.
ADCS	Magnetometer	1	2 x 2 x 0.85
	Gyro	0.142	3 x 3 x 0.9
	Sun sensor	3	3 x 3 x 1.47
	Driver circuits	1	2 x 2 x 0.5
	**Magnetorquer - rod	2.98	~35mm, diameter:3mm
	**air-core	5	35 x 35 x 2 mm
Microcontroller	arm cortex / MSP 432	1	11 x 11 x 3 mm
Peripheral Components	PCB	3	50 x 50 x 0.34
TOTAL MASS & VOLUME		94.602	51 x 46 x 6

Figure 7.31: Mass and volume budget for the femto satellite

Deployer-The Hub

Deployer-The Hub The hub serves as a deployer until the designated orbit is reached. After the femto satellites are safely deployed, a propulsion manoeuvre is conducted to place the Hub at it's orbit-792.5km

8.1 | TabSat Mission Requirements

- Most CubeSat missions employ an organization to be responsible for all mission coordination duties. That roll is usually referred to as the Mission Integrator, whose responsibilities can include coordinating safety documentation with Range Safety, interfacing with the CubeSat Developers, ICD requirement verification with CubeSat Developers and the Launch Vehicle Contractor (LVC), acting as the point of contact for licensing agencies, CubeSat to dispenser integration and testing, and coordinating with the JSpOC for pre- and post-launch identification of each CubeSat in orbit. In essence, the Mission Integrator acts as the interface between the CubeSat Developer and the LVC, and will provide the official mission requirements to the CubeSat Developer. (60)
- Although mission requirements are oftentimes similar to the requirements in the CDS, the CubeSat Developer will only be responsible for meeting the requirements provided by the Mission Integrator. The requirements in this document are meant for preliminary design purposes, and are written conservatively to allow for the best chances of compatibility with any launch vehicle.

8.2 | 6U Dispenser Interface

- The 6U Dispenser is designed to carry a standard 6U CubeSat and serve as the interface between the CubeSat and LV. Essentially, it's a rectangular box that utilizes a hinged door and spring mechanism to deploy its payload. A deployment signal sent from the LV actuates the release mechanism to open the door, and the CubeSat is ejected from the dispenser. (60)
- Multiple companies are developing 6U Dispensers which all adhere to one of two standardized constraint systems. The first is very similar to the rail system utilized by the Poly Picosatellite Orbital Deployer (P-POD), and is used on the Tyvak and Innovative Solutions In Space (ISIS) dispensers. The second system, developed by Planetary Systems Corporation (PSC), utilizes two thinner rails henceforth referred to as 'tabs' that run along the length of the CubeSat. The PSC 6U Dispenser employs a constraint mechanism that clamps onto these tabs and, when integrated, creates a stiff invariant load path.
- In both cases, the deployment force is provided by a main spring driving the internal pusher plate. The pusher plate, in turn, interfaces with the CubeSat, which glides along the 6U Dispenser rails as it's ejected into orbit. Mechanical requirements for the rail system CubeSat are outlined in Section 3.2, and the mechanical requirements for tabbed CubeSats can be found at planetarysystemcorp.com. Developers are encouraged to explore both options to determine which is optimal for their needs. Due to the mechanical differences in dispenser designs, CubeSats might not be compatible with both types of dispensers.

8.3 | Requirements

This section focuses on listing the requirements for the design and development of the Hub.

8.3.1 | General requirements

- All parts shall remain attached to the CubeSats during launch, ejection and operation. No additional space debris will be created. No pyrotechnics shall be permitted. Any propulsion systems shall be designed, integrated, and tested in accordance with AFSPCMAN 91-710 Volume 3. Propulsion systems shall have at

least 3 independent inhibits to activation. Total stored chemical energy will not exceed 100 Watt-Hours. (60)

- CubeSat hazardous materials shall conform to AFSPCMAN 91-710, Volume 3. CubeSat materials shall satisfy the following low out-gassing criterion to prevent contamination of other spacecraft during integration, testing, and launch.
- CubeSat materials shall have a Total Mass Loss (TML) < 1.0
- CubeSat materials shall have a Collected Volatile Condensable Material (CVCM) < 0.1
- The CubeSat shall be designed to accommodate ascent venting per ventable volume/area < 2000 inches.

Note: Some launch vehicles hold requirements on magnetic field strength. As a general guideline, it is advised to limit the magnetic field outside the CubeSat static envelope to 0.5 Gauss above Earth's magnetic field, while the CubeSat is integrated in the dispenser.

8.3.2 | Mechanical Requirements

- 6U CubeSats are picosatellites with dimensions and features outlined in the 6U CubeSat Specification Drawing. General features of all CubeSats without tabs include: The origin of the CubeSat coordinate system is located at the geometric center of the CubeSat. (60)
- The 6U CubeSat configuration and physical dimensions shall be per the appropriate section of the -Z face of the CubeSat will be inserted first into the 6U Dispenser.
- No components on the yellow shaded faces shall exceed 10 mm normal to the surface.
- When completing a CubeSat Acceptance Checklist (CAC), protrusions will be measured from the plane of the rails. Deployables shall be constrained by the CubeSat, not the 6U Dispenser.
- Rails shall have a minimum width of 8.5mm. Rails will have a surface roughness less than 1.6 μm . The edges of the rails will be rounded to a radius of at least 1 mm. At least 75 percent of the rail will be in contact with the 6U Dispenser rails. 25 percent of the rails may be recessed, and no part of the rails will exceed the specification. The maximum mass of a 6U CubeSat shall be 12.00 kg.

- The CubeSat center of gravity shall be located within 4.5 cm from its geometric center in the X direction, within 2 cm from its geometric center in the Y direction, and within 7 cm from its geometric center in the Z direction.
- Typically, Aluminum 7075, 6061, 6082, 5005, and/or 5052 are used for both the main CubeSat structure and the rails. If materials other than aluminum are used, the CubeSat Developer should contact the Mission Integrator or dispenser manufacturer.
- The CubeSat rails and standoff, which contact the 6U Dispenser rails and ejector plate, shall be hard anodized aluminum to prevent any cold welding within the 6U Dispenser.

8.3.3 | Electrical Requirements

- The CubeSat power system shall be at a power off state to prevent the CubeSat from activating any powered functions while integrated in the 6U Dispenser from the time of delivery to the LV through on-orbit deployment. CubeSat powered functionality includes a variety of subsystems such as Command and Data Handling (C&DH), RF Communication, Attitude Determination and Control (ADC), and deployable mechanism actuation. CubeSat power systems include all battery assemblies, solar cells, and coin cell batteries. (60)
- The CubeSat shall have, at a minimum, one deployment switch, which is actuated while integrated in the 6U Dispenser.
- The CubeSat shall include a RBF pin. The RBF pin shall cut all power to the satellite once it is inserted into the satellite.
- CubeSats shall incorporate battery circuit protection for charging/discharging to avoid unbalanced cell conditions. Additional manufacturer documentation and/or testing will be required for modified, customized, or non-UL-listed cells.
- The CubeSat shall have at least three independent RF inhibits to prohibit inadvertent radio frequency (RF) transmission. An inhibit is a physical device between a power source and a hazard. A timer is not considered an independent inhibit.

Note: Some launch vehicle providers will only require one or two independent inhibits depending on the CubeSat's RF power output. However, the use of three independent inhibits is highly recommended and can reduce required documentation and analyses.

8.3.4 | Operational Requirements

- CubeSats will meet certain requirements pertaining to integration and operation to meet legal obligations and ensure the safety of other CubeSats. These requirements are applicable for all dispensers. Dispenser specific options are available, however additional options may limit launch opportunities. (60)
- Operators will obtain and provide documentation of proper licenses for use of radio frequencies per their country's requirements.
- The CubeSat will comply with its country's radio license agreements and restrictions.
- All deployables such as booms, antennas, and solar panels shall wait to deploy a minimum of 30 minutes after the CubeSat's deployment switch(es) are activated during 6U Dispenser ejection.
- No CubeSats shall generate or transmit any RF signal from the time of integration into the 6U Dispenser through 45 minutes after on-orbit deployment from the 6U Dispenser. However, the CubeSat can be powered on following deployment from the 6U Dispenser.
- The Mission Integrator may conduct a fit check in which the CubeSat Developer hardware will be inspected and integrated into the 6U Dispenser or Test 6U Dispenser. A final fit check will be conducted prior to launch. The CubeSat Acceptance Checklist (CAC) can be used to verify compliance of the specification.

8.3.5 | Testing Requirements

Before detailing the typical CubeSat testing requirements, it is important to point out that all testing levels and requirements are mission specific and vary with every launch. The examples provided in this document, are typically, the most stringent to encompass requirements from most of the possible launch opportunities to date. (60)

- **Random Vibration**- Random vibration testing shall be performed to the levels and duration as defined by the Mission Integrator.
- **Thermal Vacuum Bakeout**- Thermal vacuum bakeout shall be performed to ensure proper outgassing of components. The test specification will be defined by the Mission Integrator.

- **Shock Testing**-Shock testing is typically not required for CubeSats. However, if necessary, shock testing shall be performed as defined by the Mission Integrator.
- **Visual Inspection**-Visual inspection of the CubeSat and measurement of critical areas will be performed per the appropriate 6U CAC.
- **CubeSat Testing Philosophy**-This section outlines a conservative test flow approach for CubeSats to meet environmental test requirements for launch. The CubeSat shall be subjected to either qualification or protoflight testing as defined in the CubeSat Testing Flow Diagram. The test levels and durations will be supplied by the Mission Integrator.

8.3.6 | Deployment and Spring Design

- **Spring design/selection:**

D(mm)	Mean Diameter
d(mm)	Wire diameter
H(mm)	Deflection
C=D/d	Spring Index
k(N/mm)	Spring Constant
Ls(mm)	Solid Length
N	Number of coils
W(N)	Load on Spring
P(mm)	pitch of coils
G(N/mm ²)	Modules of rigidity
T	Design Shear stress
Kt	Stress Factor
Sut	Ultimate Tensile strength
A	Material based value
m	constant
Tmax	Maximum value
Grad1	Tensile strength(based on d)

Table 8.1: Nomenclature of Spring

■ Deployment Velocity

F spring(N)	1250
m(total mass)(kg)	0.4
H(m)	0.03
Elastic potential Energy(J)	18.75

Table 8.2: Nomenclature of Spring

■ Using Momentum Equation

$$\text{Velocity(m/s)} \quad 9.682458366$$

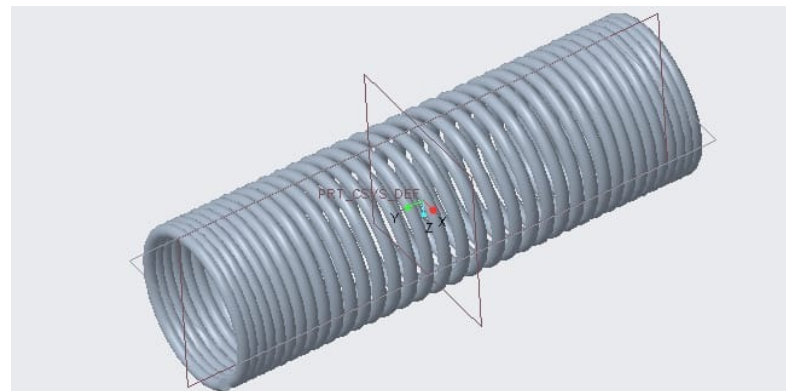


Figure 8.1: Spring

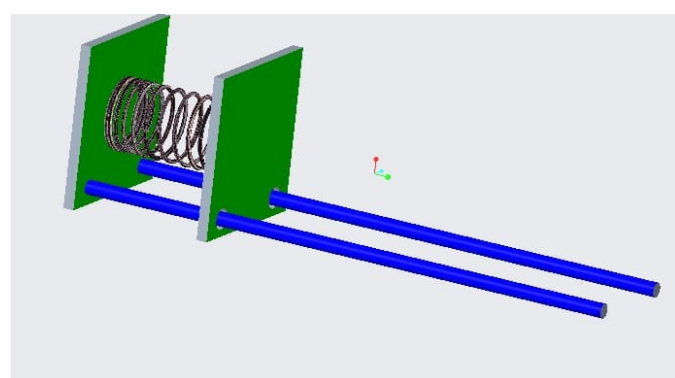


Figure 8.2: Spring Mechanism

8.3.7 | Deployment of the Solar Panels

6 U CubeSat's solar panel module with a new version of a burn wire triggering type of HRM is proposed using Nylon Wire. The proposed solar panel module with stiffener design is advantageous to guarantee the structural safety of the solar cells in accordance with the reduction of panel deflection. (62) (63)

Item	Details	Value
Nylon wire	Manufacturer	Berkley Co.
	Material	Fluorocarbon
	Diameter	0.1 mm
	Maximum allowable force	56.22 N
Burn resistor	Manufacturer	Walsin Technology Co.
	Packaging type	Surface mount device
	Package size code	3216
	Electrical resistance	4.7 Ω
	Resistance tolerance	±1%
Max. power dissipation		0.25 W ($T_{amb} = 70^{\circ}\text{C}$)

Figure 8.3: Item Specification

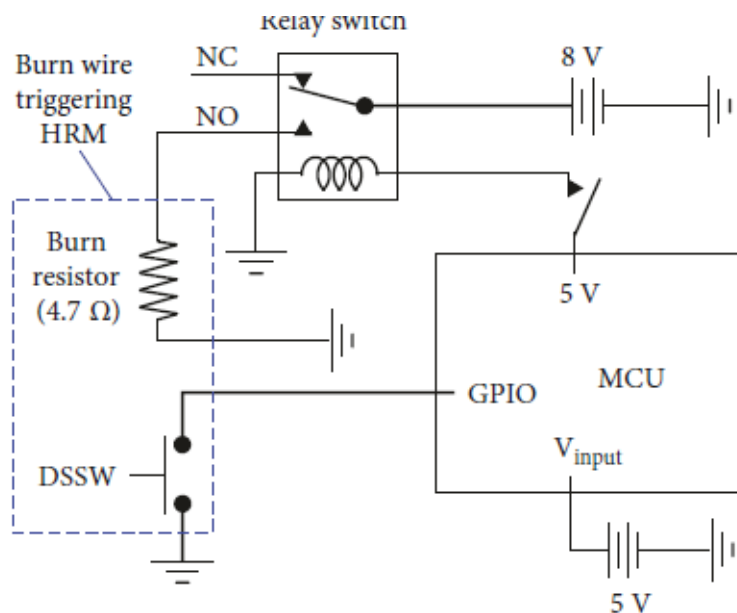


Figure 8.4: Solar panel deployment circuit

8.4 | Design Overview

- The primary mission of the 6U Deployer Program is to provide access to space for small payloads.
- The primary responsibility of companies developing 6U Dispensers is to ensure the safety of the CubeSat and protect the launch vehicle (LV), primary payload, and other CubeSats during launch. CubeSat Developers should play an active role in ensuring the safety and success of CubeSat missions by implementing good engineering practice, testing, and verification of their systems.
- Failures of CubeSats, 6U Dispensers, or interface hardware can damage the LV or a primary payload and put the entire CubeSat Program in jeopardy. As part of the CubeSat Community, all participants have an obligation to ensure safe operation of their systems and to meet the design and minimum testing requirements outlined in this document.

The following are the final designs of the Hub

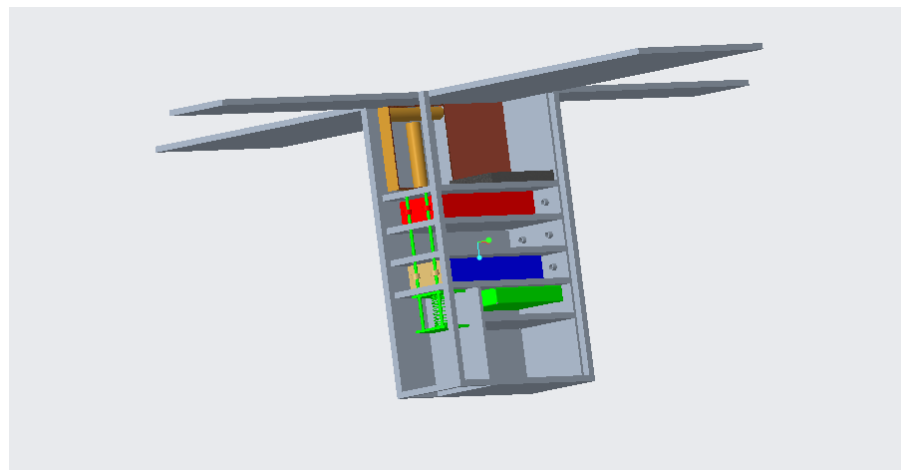


Figure 8.5: Hub Design with solar panels

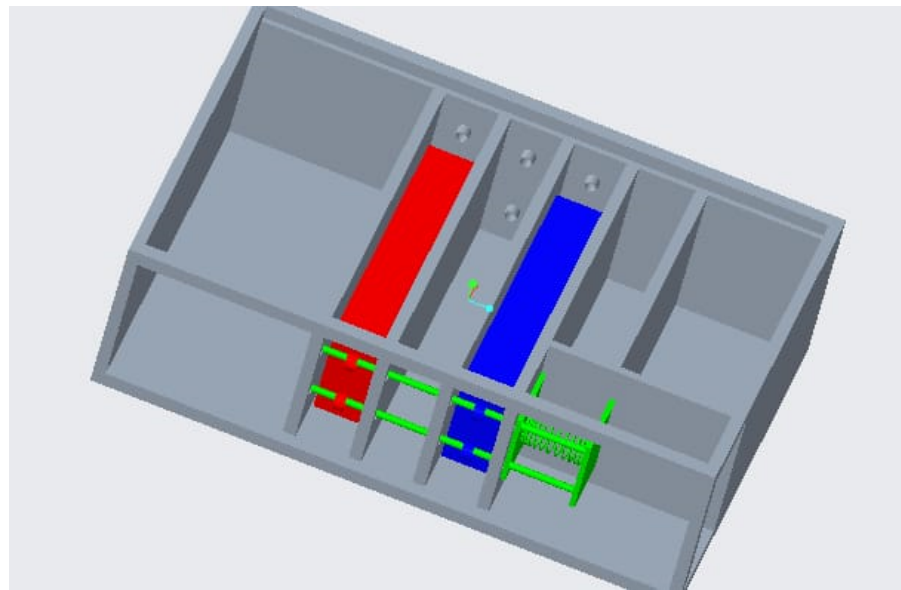


Figure 8.6: Hub Design without Solar Panels

8.4.1 | Design of Magnetic Torquers for Attitude Control

The individual components responsible for Attitude control were modelled to give an idea as to how it would placed in the Hub

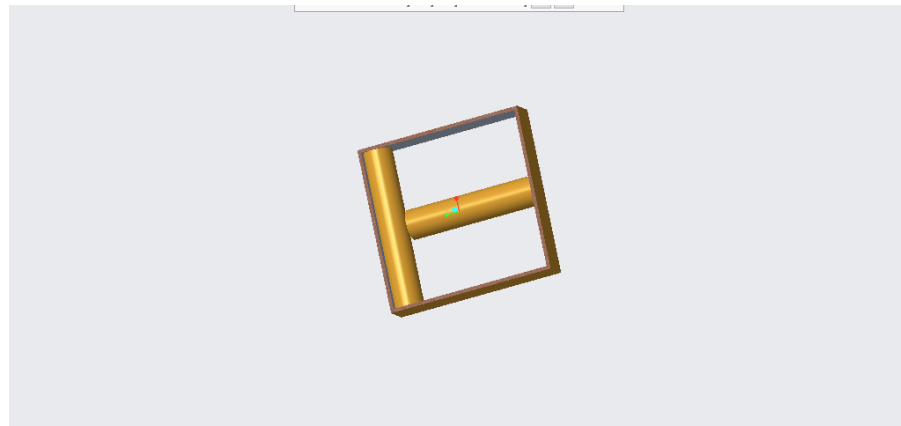


Figure 8.7: Magnetic Torquers

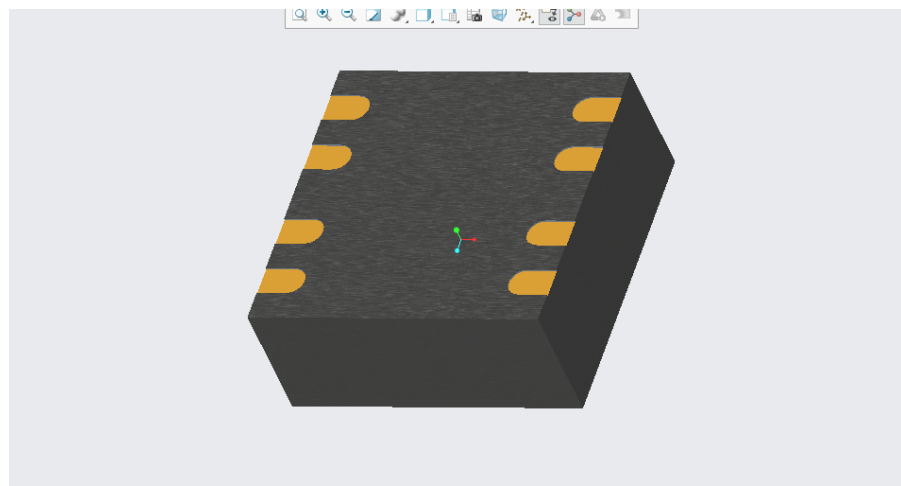


Figure 8.8: Magnetometer

8.5 | Structural Requirements

- All edges contacting rails must be rounded.
- Cubesats must have at least 75 percent (85.125 mm of a possible 113.5 mm) of flat rail contact with the deployer. To prevent cold-welding, raw metal is not allowed as the contact surface of the bottom standoff.
- Derlin inserts, or a hard anodize are examples of acceptable contact surfaces.
- The outer surfaces of the CubeSats are required to be hard anodized in order to prevent wear between the sliding rails and the CubeSats.
- Separation springs (SSMD-51P recommended) must be included at designated contact points. A custom separation system may be used.
- One deployment switch is required (two are recommended) for each CubeSat.

Here are structural parameters considered during the 6U Hub Design: (64)

Symbol	Parameter	Conditions	Unit	Min	Max	Min	Max	Min	Max
TL (1)	Tab Load	directional RSS of quasi-static or 3σ random vibration, at payload tabs	N [lb]	- [800]	3559 [800]	- [800]	3559 [800]	- [800]	3559 [800]
CMX	Center of mass, X	Stowed in CSD	mm [in]	-20 [-.79]	20 [.79]	-40 [-1.57]	40 [1.57]	-40 [-1.57]	40 [1.57]
CMY	Center of mass, Y	Stowed in CSD	mm [in]	10 [.39]	70 [2.76]	10 [.39]	70 [2.76]	55 [2.17]	125 [4.92]
CMZ	Center of mass, Z	Stowed in CSD	mm [in]	133 [5.24]	233 [9.17]	133 [5.24]	233 [9.17]	133 [5.24]	233 [9.17]
Height	Maximum payload depth, +Y dimension		mm	-	109.7	-	109.7	-	222.8
			[in]		[4.319]		[4.319]		[8.772]
Width	Maximum payload width from origin, ±X dimension		mm [in]	-	56.55 [2.226]	-	119.7 [4.713]	-	119.7 [4.713]

Tab	±X dimension		mm	112.7	113.1	239	239.4	239	239.4
Width			[in]	[4.437]	[4.453]	[9.409]	[9.425]	[9.409]	[9.425]
Tab	+Z dimension		mm	361	366	361	366	361	366
Length			[in]	[14.21]	[14.41]	[14.21]	[14.41]	[14.21]	[14.41]
EP _Y	Ejection plate contact zone, +Y dimension from origin		mm [in]	- [3.94]	100 [3.94]	- [3.94]	100 [3.94]	- [3.94]	213 [8.39]
DC_X1	Deployable contact zone w ith CSD, ±X face near +Y face		mm [in]	91.4 [3.598]	- [3.598]	91.4 [3.598]	- [3.598]	204.5 [8.051]	-
DC_X2	Deployable contact zone w ith CSD, ±X face near -Y face		mm [in]	- [0.799]	20.3 [0.799]	- [0.799]	20.3 [0.799]	- [0.799]	20.3 [0.799]
DC_+Y	Deployable contact zone w ith CSD, +Y face (2)		mm [in]	43.85 [1.726]	- [4.213]	107 [4.213]	- [4.213]	107 [4.213]	-

DC_-Y	Deployable contact zone w ith CSD, -Y face (2)		mm [in]	31.2 [1.228]	-	94.3 [3.713]	-	94.3 [3.713]	-
r _{DS}	Force from optional deployment sw itches, summated, Z axis (3)	When contacting CSD ejection plate. Per CSD ejection Spring.	N	-	5	-	5	-	5
r _{DS}	Payload separation from ejection plate								
r _{DS}	necessary to change deployment sw itch	If sw itches reside on -Z face.	mm [in]	1.3 [.05]	12.7 [.50]	1.3 [.05]	12.7 [.50]	1.3 [.05]	12.7 [.50]
r _{FD}	Friction force deployables impart on CSD walls during ejection	summated (all 4 sides), per CSD ejection spring	N	-	2	-	2	-	2
TML	Total Mass Loss	Per ASTM E 595-77/84/90	%	-	1	-	1	-	1
CVCM	Collected Volatile Condensable Material	Per ASTM E 595-77/84/90	%	-	0.1	-	0.1	-	0.1
DP	CSD de-pressurization rate	During launch	psi/s	-	1	-	1	-	1

D _X	Location of optional separation electrical connector, +X dimension		mm [in]	40.67 [1.601]	41.17 [1.621]	103.84 [4.088]	104.34 [4.108]	103.84 [4.088]	104.34 [4.108]
----------------	--	--	------------	------------------	------------------	-------------------	-------------------	-------------------	-------------------

8.6 | Material

Aluminum 7075 or 6061-T6 is suggested for the main structure. If other materials are used, the thermal expansion coefficient must be similar to that of Anodized Aluminum 7075-T3. Properties

■ Corrosion Resistant

- Avoiding stay light in optical equipment
- Scratch Resistant
- Good Surface finish
- Low weight as compare to other.

Structure	Dimensions (mm)	Primary Structure Mass (kg)	Primary + Secondary Structure Mass (kg)	TRL Status
1U	100 x 100 x 114	0.1	0.2	9
2U	100 x 100 x 227	0.16	0.2	9
3U	100 x 100 x 341	0.24	0.3	9
6U	100 x 226 x 340.5	0.9	1.1	9
8U	226 x 226 x 227	1.3	1.9	Unkn.
12U	226.3 x 226 x 341	1.5	2.0	7

Figure 8.9: Dimensions of 6U structure

8.7 | Analysis

The Hub requires certain analysis in order to validate the design.

8.7.1 | Dynamical Analysis

Dynamical Analysis is used to predict Design Limit Load. The maximum structural loading typically results from the dynamic response during random vibration testing and/or shock testing. These loads are dependent on the mass, stiffness, and damping properties unique to each payload. The method below provides a rudimentary means of predicting these loads. (64) Steps involved-

1. Create a simplified model of the payload consisting of the primary structure and significant components for a Normal Modes Analysis from 20-2,000Hz.
2. Identify the dominant resonant frequencies and mode shapes for each orthogonal direction (X, Y, Z). These modes can be identified as having the highest percentage of Modal Effective Mass relative to all modes modeled within the frequency bandwidth stated above.

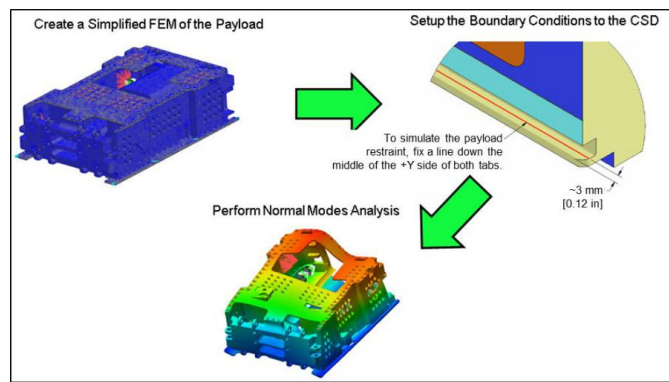


Figure 8.10: Steps involved in Dynamical Analysis

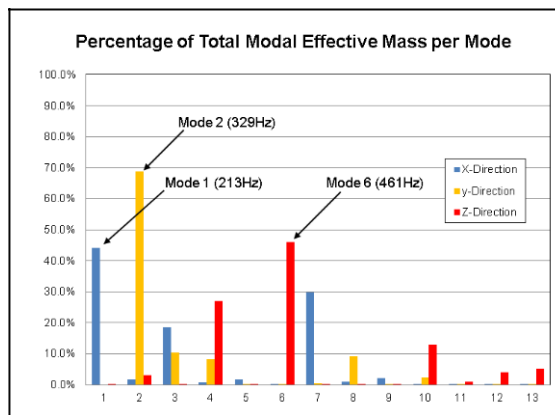


Figure 8.11: Modal Analysis

3. The response for a random vibration profile can be predicted by using the Miles Relation shown below:

8.7.2 | Electromagnetic Interference Analysis

This section addresses the potential magnetic interference generated by the magnetic torquers used for attitude determination and control (ADC) in Femoyer Mission. (62)

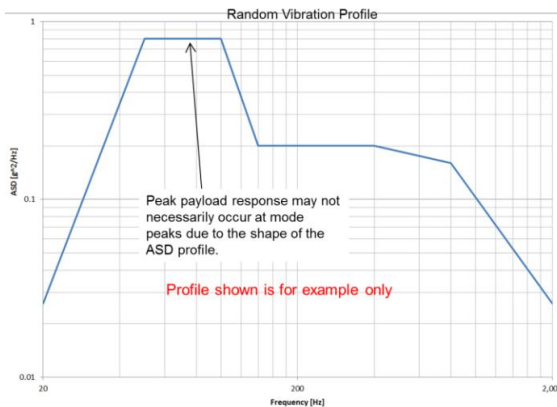


Figure 8.12: Random Vibration Profile

8.7.3 | Impact of Magnetic Torquer on the Magnetometer

The protection of the magnetometer from residual magnetic fields is of utmost importance for our mission's success. There are three options for magnetometer location:

- Inside middle unit of CubeSat
- On a deployable boom
- Surface mount

However, the magnetic field resulting from three magnetic torquers poses a risk of interference with the magnetometer's ability to record the ambient magnetic field of Earth.

A deployable boom is also an option for mounting our magnetometer. Several designs will be discussed later on. Certain structural considerations are necessary to determine when to deploy the boom. Furthermore, the communication between the magnetometer and the on-board computer is more complicated with a deployable boom due to the magnetometer's distance and angle from the Hub. The most realistic option is mounting the magnetometer on the surface of the Hub. This will allow the magnetometer to get readings from Earth's ambient magnetic field while still maintaining a safe distance away from the magnetic field generated by the actuation of the magnetic torquers. Magnetically insulating material could rest between the mounted magnetometer and the aluminum shell of the Hub. This material would ensure no electromagnetic interference between the instrumentation within the Hub and the magnetometer mounted outside the Hub.

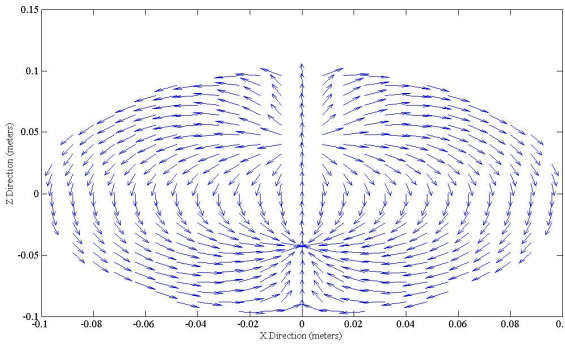


Figure 8.13: Magnetic field lines from a single magnetic torquer shown moving along central axis and ‘spilling over’ to the sides at the top

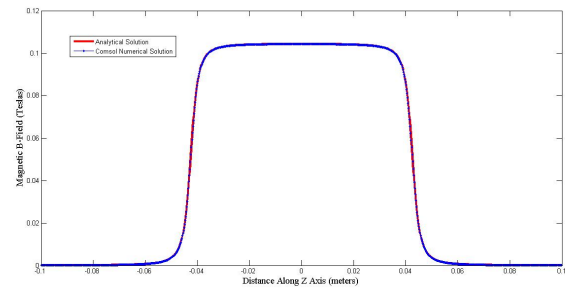


Figure 8.14: Magnetic B field of a magnetic torquer modeled as a solenoid

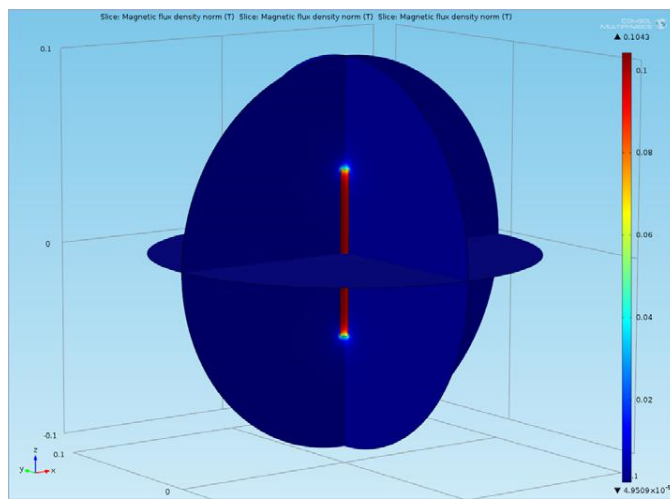


Figure 8.15: Multiphysics numerical simulation of a single magnetic torquer in free space

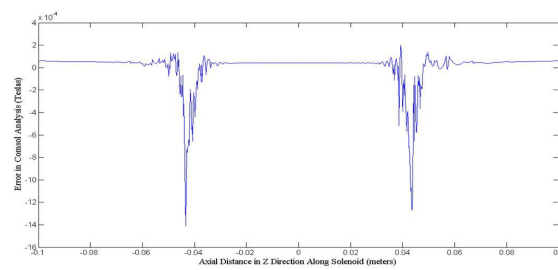


Figure 8.16: Error of numerical computation when compared to analytical solution

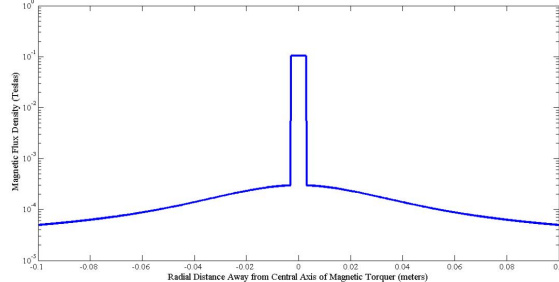


Figure 8.17: B field values for a single magnetic torquer versus the radial distance away from the central axis of the magnetic torquer.

Propulsion Subsystem

9.1 | Micro-propulsion system for HUBsat

In the proposed design of constellation of femtosatellites, Deployer will be responsible to deploy femtosatellite in trailing formation and after the deployment it will be working as HUB satellite for communication purpose to the ground station. To keep pace with all femtosatellite, orbital altitude of the HUB satellite will be raised by 500 meters in same orbital plane. This operation will be done by Hohmann transfer orbit maneuver; this is where the need of propulsion system (7) arises.

Factors affecting the selection of Propulsion system:

- Thrust to Weight ratio
- Power requirement
- Propellant type and mass
- Space required and Size
- Max. Delta V
- Reliability
- Control interface
- Operating temperature
- Total and specific impulse

Considering all of this main constraints we selected VACCO's Propulsion Unit for CubeSats (PUC) (8). It is a delta-V propulsion system specifically optimized for CubeSats. The PUC is available in a variety of sizes from 0.14U to 1U. Features include minimal payload displacement, high delta-V, low mass, low power and a simple control interface. Development hardware has been extensively tested including 75,000+ cold gas firings in a vacuum chamber. The self-contained PUC includes an integral controller, propellant storage, propellant feed system, sensors and a 4.4 mN warm gas thruster. Reliability is ensured through simplicity of design, welded titanium construction and friction less valve technology (9).

Features:

- Scalable from 0.14U (shown) to 1U
- Minimal Payload Displacement
- High Total Impulse and Delta-V
- 4.4 mN Warm Gas Thruster
- Extremely Low Power
 - 5.3 watts in Warm Gas Mode
 - <1 watt in Cold Gas Mode
 - Zero Power when not Firing
- Simple Control Interface
- Reliable, Friction less Valve Technology

Table 9.1: Performance matrix

Tank Vol (cm ³)	Total Impulse (N-Sec)	Specific Impulse (Sec)	Wet mass (grams)	Dry Mass (grams)	Total mass (mN)	Thrust (mN)
190	213	92	200	406	606	4.4

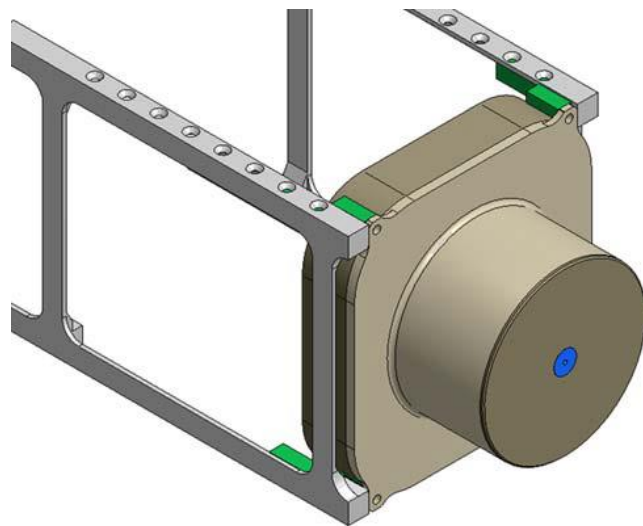


Figure 9.1: Propulsion Unit for CubeSats (PUC) Mounted on Cubesat structure

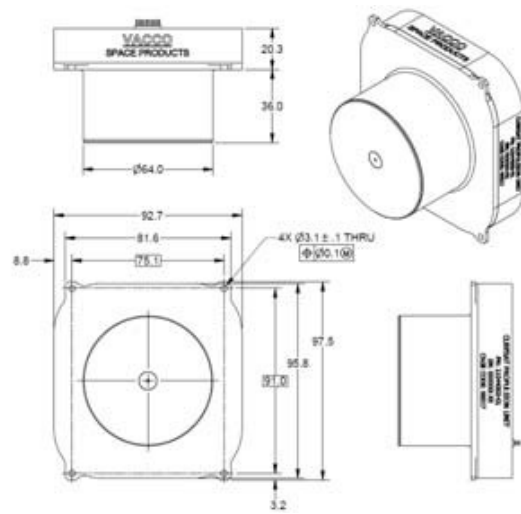


Figure 9.2: Dimensions of Propulsion Unit for CubeSats (PUC) - 0.14U

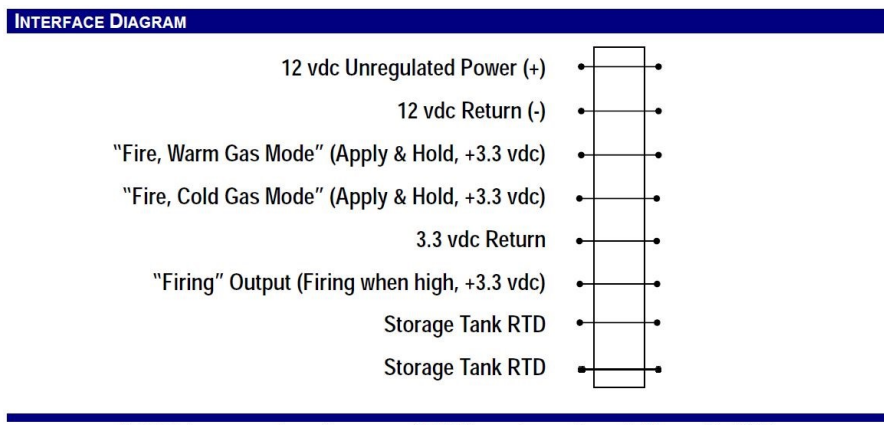


Figure 9.3: Interface Diagram

Conclusion

This report presents a theoretical design approach of a distributed system of femtosatellite and a femtosatellite deployer to monitor the progress of forest fires. The increasing incidences of unanticipated forest fires are a growing cause of imbalances in various aspects of the biosphere. This poses a threat to the ecosystem and fuels many problems such as global warming, reduction in vegetation, air pollution, habitat destruction, etc. The use of satellites to detect forest fires at the earliest possible time helps avoid unwanted negative effects of such disasters. Due to their small size and cost, femtosatellites in particular have great potential in preventing disasters. The TabSat equipped with imaging payload and ADCS (Magnetorquers, Gyroscope, Magnetometer and Sun sensor) is effective in monitoring and imaging applications. The femto satellite hub and the deployer are both contained in a 6U CubeSat structure along with a proposed propulsion system. The use of an imaging payload and ADCS on the PCB of the femtosatellite highlights the significance of the TabSat, simultaneously pointing towards the implementation of more efficient trade-offs between parameters such as cost and weight, for the upcoming mission advancements.

10.1 | Achieved Aims and Objectives

The femtosatellite, along with its components and payload, were modeled in a CAD software to enact its spacial orientation across the PCB. The goal of the project was to enable the femtosatellite for forest fire monitoring by employing an image sensor. The power budget depicted in above sections elaborates the management of power and ensures unhindered performance, which would otherwise arise mostly due to power insufficiency. In order to supply the satellite with sufficient operating power, a coin battery is employed along with solar panels. The Sun-Synchronous Polar Orbit was

selected to ensure the continuous functioning of the femtosatellite as it avoids eclipses. The power system was designed to avoid power loss to the sensors and payload, as it would otherwise result in loss of data and a subsequent failure of the mission. The orbit was designed and simulated over the target area to envision the mission.

10.2 | Critiques and limitations

Although the TabSat was designed to position itself at the target area and monitor it, uncertainty always manages to manifest itself in ways it becomes impossible to anticipate the shortcomings of the mission. There is limited data about the noise which would arise from different sources such as the space itself. Another source of noise is the atmosphere. As the TabSat uses the visible range of radiation to detect forest fires, clouds in the lower atmosphere can mask the fires and prevent us from detecting their progress. However, some parameters such as smoke from the fire may also be an excellent indicator of the disaster.

10.3 | Future Work

In recent years, the increase in research related to femtosatellites has opened a new gate-way of cost effective and short lived remote sensing for Earth observation. Although, there have been a few instances of successful execution of missions involving femtosatellites, their full potential still remains unknown. That said, it's imperative to note that their actual limits seems yet to be exploited in the form of inter-planetary exploration missions. While many designs and mission concepts have been proposed for Earth, using femtosatellites in interplanetary missions has yet to be attempted. All femtosatellite designs face similar challenges i.e., housing of essential subsystems (power, communication, data handling, and payload) on a PCB board or integrated chip. Due to their size and significantly low inertia, the femtosatellites stand a chance to survive an atmospheric re-entry, allowing a tremendous opportunity to study the atmospheric properties in the lower altitude orbits of other planets. Keeping aside the structural aspect of such femtosatellite designs, the most crucial aspect becomes the radio transmission of data. There will be a strong need to use signal noise reduction techniques using filters to avoid signal interruptions. Careful selection of orbit and trajectories remain one of the most uncertain segments of mission planning. An extensive analysis on thermal constraints of the femto satellite would pave way to decide on the thermal control system that can be incorporated. A complete simulation of the ADC (Attitude

Determination and Control) system would give a better idea about the pointing accuracy and other intricacies involved in the system.

Moving forward, a predictive approach to our mission could be implemented for the detection of natural disasters and for the classification of important data at the hub.

However, the nearest advancements in this field will require the femtosatellite to be equipped with systems similar to their conventional counterparts, but still satisfy the weight constraints to categorize itself as a “Femtosatellite”.

References

- [1] <https://spacenews.com/are-small-satellites-the-solution-for-space-weather-monitoring/>
- [2] https://en.wikipedia.org/wiki/Small_satellite#:~:text=Miniaturizedsatellitesallowforcheaper,forlowdataratecommunications
- [3] <https://ui.adsabs.harvard.edu/abs/2016PhDT.....163P/abstract>
- [4] J. Tristanco and J. Gutierrez-Cabello, " A Probe of Concept for FEMTO-SATELLITES based on Commercial-Of-The-Shelf", Digital Avionics Systems Conference (DASC), 2011 IEEE/AIAA 30th , Seattle, Washington, USA , pp: 8A2-1 - 8A2-9, 16-20 October 2011.
- [5] <https://smallwarsjournal.com/jrn1/art/a-small-box-that\T1\textquoterights-\a-big-deal-how-latin-american-countries-are-using-\cubesats-and-why-it-ma>
- [6] <https://digitalcommons.usu.edu/smallsat/2013/all2013/111/>
- [7] Analysis, Fabrication and Testing of a MEMS-based Micropropulsion System
- [8] <https://cubesat-propulsion.com/propulsion-unit/>
- [9] Micropropulsion system selection for precision formation flying satellites Jeffrey Reichbach, Raymond Sedwick and Manuel Martinez-Sanchez
- [10] https://en.wikipedia.org/wiki/Sun-synchronous_orbit
- [11] https://en.wikipedia.org/wiki/Sun-synchronous_orbit#/media/File:Heliosynchronous_orbit.svg

- [12] "State of the Art Small Spacecraft Technology" by Small Spacecraft Systems Virtual Institute
- [13] https://aisolutions.com/_freeflyeruniversityguide/hohmann_transfer.htm#calculatinghohmanntransfers"A novel concept for earth remote sensing using a bi-static
- [14] femto-satellite swarm in sun synchronous orbit" by Jianlin Cao, Deepak Uttam-chandani.
- [15] A probe of concept for femto-satellites based on commercial-of-the-shelf, Joshua Tristancho, Jordi Gutiérrez, Universitat Politècnica de Catalunya
- [16] Design and implementation of a femto-satellite technology demonstrator by Victor Kravchenko
- [17] Study of Current Femto-Satellite Approches and Services, Nizar Tahri,Chafaa Hamrouni, Adel M.Alimi, REGIM-Lab: Research Groups on Intelligent Machines, Department of Electrical Engineering, National Engineering School of Sfax (ENIS)
- [18] A Case Study in Femtosatellite Communications by Alex Akins
- [19] Implementation of a femto-satellite and a mini-launcher Joshua Tristancho SUPERVISED BY Jordi Gutierrez Universitat Politècnica de Catalunya Master in Aerospace Science & Technology May 2010
- [20] <https://www.heavens-above.com/orbit.aspx?satid=32382>
- [21] KickSat: A Crowd-Funded Mission to Demonstrate the World's Smallest Spacecraft Zachary Manchester, Cornell University Mason Peck, Cornell University Andrew Filo, 4Special Projects
- [22] Walter Hohmann, Die Erreichbarkeit der Himmelskörper, Oldenbourg, Munich, 1925. Also, The Attainability of Heavenly Bodies, NASA Technical Translation F-44, 1960.
- [23] Jean-Pierre Marec, Optimal Space Trajectories, Elsevier, 1979.
- [24] R. P. Brent, Algorithms for Minimization Without Derivatives, Prentice-Hall, 1972
- [25] R. H. Battin, An Introduction to the Mathematics and Methods of Astrodynamics, AIAA, 1987.

- [26] D. F. Lawden, Optimal Trajectories for Space Navigation, Butterworths, London, 1963.
- [27] John E. Prussing, "Simple Proof of the Global Optimality of the Hohmann Transfer", AIAA Journal of Guidance, Control and Dynamics, Vol. 15, No. 4.
- [28] "Space mission analysis and design," Choice Reviews Online, vol. 29, no. 09, pp. 29-5149-29–5149, May 1992, doi: 10.5860/CHOICE.29-5149.
- [29] L. Yang, J. Guo, C. Fan, X. Song, S. Wu, and Y. Zhao, "The design and experiment of stardust femto-satellite," Acta Astronautica, vol. 174, pp. 72–81, Sep. 2020, doi: 10.1016/j.actaastro.2020.04.034.
- [30] G. McVittie and K. Kumar, "Design of a COTS Femtosatellite and Mission," presented at the AIAA SPACE 2007 Conference & Exposition, Long Beach, California, Sep. 2007, doi: 10.2514/6.2007-6034.
- [31] D. J. Barnhart, T. Vladimirova, A. M. Baker, and M. N. Sweeting, "A low-cost femtosatellite to enable distributed space missions," Acta Astronautica, vol. 64, no. 11–12, pp. 1123–1143, Jun. 2009, doi: 10.1016/j.actaastro.2009.01.025
- [32] N. Tahri, C. Hamrouni, and A. M. Alimi, "Study of Current Femto-Satellite Approaches," International Journal of Advanced Computer Science and Applications (IJACSA), vol. 4, no. 5, 36/01 2013, doi: 10.14569/IJACSA.2013.040520.
- [33] N. Aidynbay, "Mission analysis for a swarm of femtosatellites to study the lower thermosphere," Feb. 2020, Accessed: Oct. 07, 2020. [Online]. Available: <https://upcommons.upc.edu/handle/2117/179469>.
- [34] J. Cao, C. Clemente, C. R. McInnes, and J. J. Soraghan, "Solar Radiation Pressure Enabled Femtosatellite Based Earth Remote Sensing," IEEE Trans. Aerosp. Electron. Syst., pp. 1–1, 2020, doi: 10.1109/TAES.2020.2972242.
- [35] A. Hemadeh, K. Satyanarayana, M. El-Hajjar and L. Hanzo, "Millimeter-Wave Communications: Physical Channel Models, Design Considerations, Antenna Constructions, and Link-Budget," in IEEE Communications Surveys & Tutorials, vol. 20, no. 2, pp. 870-913, Secondquarter 2018, doi: 10.1109/COMST.2017.2783541.
- [36] Development of a 10g Femto-satellite with Active Attitude Control, Zhongxu Hu
- [37] Boscolo Fiore, "CubeSat attitude control system," Politecnico di Milano, 2020, doi: 10.13140/RG.2.2.18435.25125.

- [38] Stuurman, Bryan, "Design And Development Of Ryerson Femtosatellite" (2009). Theses and dissertations. Paper 1197
- [39] Niccolò Bellini, Prof. Jordi Puig-Suari, Prof. Paolo Tortora Magnetic Actuators for Nanosatellite Attitude Control, Anno Accademico 2013/2014
- [40] John Amin* and E. Glenn Lightsey , The Design, Assembly, and Testing of Magnetorquers for a 1U CubeSat Mission, Georgia Institute of Technology, Atlanta, GA, 30332
- [41] Stephan Theil, Pontus Appel, Alexander Schleicher, Low Cost, Good Accuracy - Attitude Determination Using Magnetometer and Simple Sun Sensor, Center of Applied Space Technology and Microgravity (ZARM), University of Bremen, 2003
- [42] Book of Abstracts, 4th European CubeSat Symposium, 30 January – 1 February 2012, Ecole Royale Militaire, Brussels
- [43] B. Ibrahim, "Study and Analyze the Attitude Determination and Control Subsystem ADCS of a Small Remote Sensing Satellite," figshare, 2020, doi: 10.6084/M9.FIGSHARE.12389300.
- [44] N. Tahri, C. Hamrouni, and A. M. Alimi, "Study of Current Femto-Satellite Approches," IJACSA, vol. 4, no. 5, 2013, doi: 10.14569/ijacsa.2013.040520.
- [45] David Vidal - Three-axes attitude determination and control system based on magnetorquers for small satellites
- [46] Attitude Determination and Control- <http://www.ece3sat.com/cubesatmodules/adcs/>
- [47] Master's Thesis Attitude determination for the Norwegian student satellite nCube by Stian Søndersrød Ose Department of Engineering Cybernetics, Norwegian University of Science and Technology Trondheim Norway June 07, 2004
- [48] D. Faizullin, K. Hiraki, HORYU-IV Team, and Mengu Cho, "Improvement Of Sun Angle Accuracy From In-Orbit Data Of A Quadrant Photodiode Sun Sensor," Zenodo, Jun. 2017, doi: 10.5281/ZENODO.583886.
- [49] V. Carrara, R. B. Januzzi, D. H. Makita, L. F. de P. Santos, and L. S. Sato, "The ITASAT CubeSat Development and Design," J. Aerosp. Technol. Manag., vol. 9, no. 2, pp. 147–156, Apr. 2017, doi: 10.5028/jatm.v9i2.614.
- [50] A Solar Cell Based Coarse Sun Sensor for a Small LEO Satellite Attitude Determination, Journal of power electronics 9(4), July 2009

- [51] Attitude Determination and Control of Future Small Satellites H. Ersin Soken, A. Rustem Aslan and Chingiz Hajiyev Aeronautics and Astronautics Faculty Istanbul Technical University Istanbul, TURKEY (PDF) Attitude Determination and Control of Future Small Satellites. Available from: https://www.researchgate.net/publication/261252726_Attitude_Determination_and_Control_of_Future_Small_Satellites [accessed Oct 13 2020].
- [52] Joshua Tristancho, Implementation of a femto-satellite and a mini-launcher, Universitat Politecnica de Catalunya, Master in Aerospace Science Technology, May 2010
- [53] Tracie R. Perez and Kamesh Subbarao, A Survey of Current Femtosatellite Designs, Technologies, and Mission Concepts, Perez, T. et al. (2016): JoSS, Vol. 5, No. 3, USA
- [54] Small Spacecraft Systems Virtual Institute Ames Research Center, Moffett Field, National Aeronautics and Space Administration, State of the Art Small Spacecraft Technology, Edition – December 2018, California
- [55] Talini Pinto Jayawardena , Commercial CubeSat missions: why GNSS testing with a simulator is essential, March 26, 2020
- [56] Narayan Prasad, An overview of GPS receivers for small satellites, Satsearch, Nov 12, 2019
- [57] Henk Key and Mathias lemmens, GPS: Position, time and distance, July 09, 2005
- [58] Stefan Söderholm1 Mohammad Zahidul H. Bhuiyan1 Sarang Thombre1 Laura Ruotsalainen1 Heidi Kuusniemi1, A multi-GNSS software-defined receiver: design, implementation, and performance benefits, 18 May 2016, Ann. Telecommun. (2016) 71:399–410 DOI 10.1007/s12243-016-0518-7
- [59] TRAIL DEPLOYER
- [60] 6U Cubesat Design Specification. PROVISIONAL. The CubeSat Program, Cal Poly SLO. CP-CDS-PROVISIONAL
- [61] Design and Analysis for a CubeSat Mission. Celena Dopart et al. Project Number: NAG-1102.
- [62] Development of Pogo Pin-Based Holding and Release Mechanism for deployable Solar Panel of CubeSat. Shankar Bhattarai et al. International

Journal of Aerospace Engineering, Volume 2019, Article ID 2580865,
<https://doi.org/10.1155/2019/2580865>

- [63] Development of 6U CubeSat's Deployable Solar Panel with Burn Wire Triggering Holding and Release Mechanism. Tae-Yong Park et al. International Journal of Aerospace Engineering, Volume 2019, Article ID 7346436, <https://doi.org/10.1155/2019/7346436>
- [64] This is a standalone specification intended for payload designers. Planetary Systems Corporation does not design or manufacture payloads. Dr. Andrew Kalman et al. www.planetarysys.com